HHS Public Access

Author manuscript

Dev Cell. Author manuscript; available in PMC 2024 April 24.

Published in final edited form as:

Dev Cell. 2023 April 24; 58(8): 645–659.e4. doi:10.1016/j.devcel.2023.03.008.

Heterodimerization-dependent secretion of Bone Morphogenetic Proteins in *Drosophila*

Milena Bauer[1,*], **Gustavo Aguilar**[1,*], **Kristi A. Wharton**[2], **Shinya Matsuda**[1], **Markus Affolter**[1,†]

[1]Biozentrum, University of Basel, Spitalstrasse 41, 4056 Basel

[2]MCB Department, Brown University, Providence, RI 02912

Summary

Combinatorial signaling is key to instruct context-dependent cell behaviors. During embryonic development, adult homeostasis and disease, Bone Morphogenetic Proteins (BMPs) act as dimers to instruct specific cellular responses. BMP ligands can form both homo- or heterodimers; however, obtaining direct evidence of the endogenous localization and function of each form has proven challenging. Here, we make use of precise genome editing and direct protein manipulation via protein binders to dissect the existence and functional relevance of BMP homo- and heterodimers in the *Drosophila* wing imaginal disc. This approach identified *in situ* the existence of Dpp (BMP2/4)/Gbb (BMP5/6/7/8) heterodimers. We found that Gbb is secreted in a Dpp-dependent manner in the wing imaginal disc. Dpp and Gbb form a gradient of heterodimers whereas neither Dpp nor Gbb homodimers are evident under endogenous physiological conditions. We find that the formation of heterodimers is critical for obtaining optimal signaling and long-range BMP distribution.

In Brief

Bone Morphogenetic Proteins (BMPs) can potentially form both hetero- or homodimers. Bauer and Aguilar et al. identify that, in the *Drosophila* imaginal wing disc, heterodimers are the only secreted and fully active ligand species. In this tissue, the secretion of Gbb depends on its heterodimerization with Dpp.

Graphical Abstract

For correspondence: markus.affolter@unibas.ch, shinya.matsuda@unibas.ch.

*These authors contributed equally.

†Lead contact

Author contributions

Conceptualization, M.B, G.A., S.M. and M.A. Investigation, M.B, G.A.; Writing – Original Draft, M.B. and G.A.; Writing – Review & Editing, K.W., S.M. and M.A.; Funding Acquisition, S.M. and M.A.; Resources, K.W and S.M.; Supervision, S.M. and M.A.

Declaration of interests

The authors declare no competing interests.

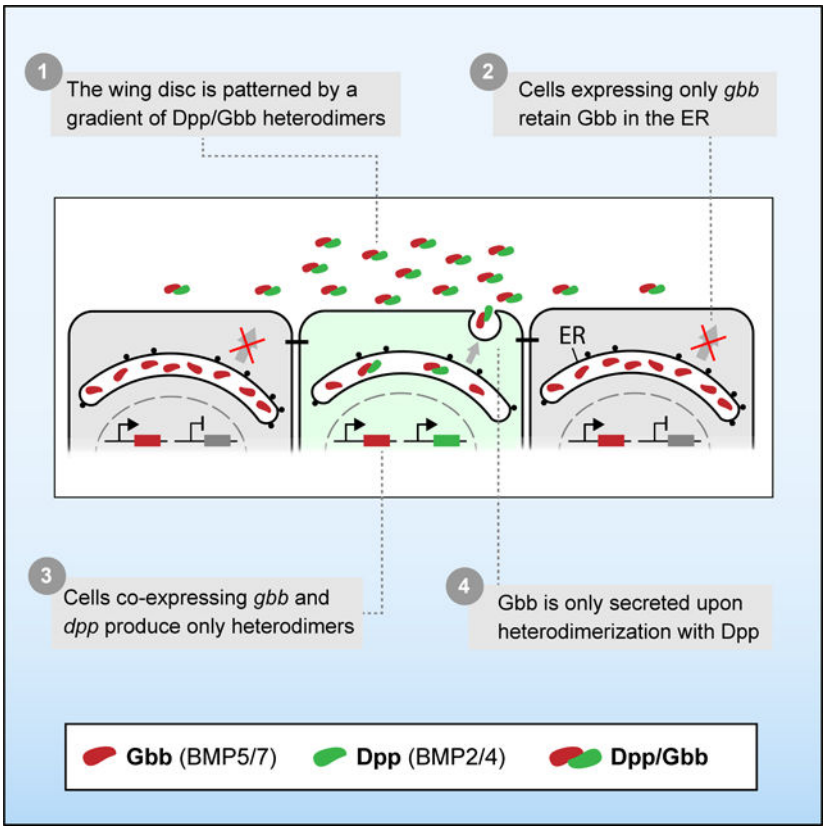

Keywords

Heterodimer; BMP; Drosophila; Protein Binders; CRISPR

Introduction

Bone morphogenetic proteins (BMPs) represent an ancient group of signaling ligands [1]. BMPs belong to the TGF-ß superfamily and have been shown to trigger cell division, differentiation and death, among other cell behaviors [2,3]. BMPs are essential regulators of the embryonic development of all metazoans. In fact, loss of BMP signaling invariably results in embryonic lethality [4,5]. BMPs are also tightly linked to several human diseases, such as cancer, where they have been described both as oncogenes and tumor suppressors [6].

During their biogenesis, pairs of BMP monomers form a disulfide bridge in the endoplasmic reticulum (ER), resulting in a covalently bound dimer. Secreted BMP dimers then act on target cells via the assembly of heterotetrameric complexes comprised of two type I and two type II Serin/Threonine kinase receptors [7]. Recognition of the BMP ligand at the surface of the cell results in type I receptor activation and downstream target gene modulation via phosphorylation of the Smad signal transducer (Mad in *Drosophila*).

In vivo, multiple BMP genes are often expressed by the same cell, potentially leading to the formation of different homo- and heterodimers. In most cases, the responding cells can

also display different type I and type II receptors. Given that different BMPs have distinct affinities for specific receptors, hetero- and homodimers can result in the formation of unique receptor complexes exhibiting diverse signaling capacities [7]. The multimeric essence of the BMP pathway elements results in a broad combinatorial space, permitting a wide range of signaling outputs depending on the context [8].

Despite their importance, the considerable diversity and redundancy of BMP ligands, coupled with the limitations of current genetic tools, has made it difficult to dissect *in vivo* both the presence and the function of BMP homodimers versus heterodimers.

In contrast to mammals, where more than 20 BMP-encoding genes have been described, the *Drosophila melanogaster* genome harbors only three genes: *decapentaplegic (dpp)*, encoding the vertebrate BMP2/4 ortholog, and screw (scw) and *glass bottom boat (gbb)*, encoding BMP5/6/7/8 orthologs. In the embryo, Dpp/Scw heterodimers are thought to be largely responsible for mediating dorsoventral patterning [9]. Indeed, Dpp requires Scw to achieve a normal extracellular distribution [9,10]. Nonetheless, localized expression of Scw or Dpp homodimers in the early embryo are each able to activate signaling at similar levels to the heterodimer [10,11]. Direct evidence of heterodimer formation remains missing.

In the larval wing precursor tissue, the wing imaginal disc, both *dpp* and *gbb* have been shown to be involved in patterning and growth [12–14]. In this tissue, *dpp* is eventually expressed in a stripe of cells along the antero-posterior axis. From there, it has been proposed that the protein forms a gradient that instructs concentration-dependent gene expression and ensures tissue growth [15,16]. Loss of *dpp* in the wing disc results in wing patterning defects and significant tissue loss [17–20]. In contrast, loss of *gbb* in the wing disc results in patterning defects and mild tissue loss that differ in part from the phenotypes displayed by the loss of *dpp* [14], suggesting different but potentially overlapping roles during wing development [21].

For both *Drosophila* and vertebrates, genetic manipulation of individual BMP genes has been used to address the relative contribution of different dimer types. However, such manipulations change the dosage of the different homo- and heterodimers relative to one another. Given the ability of different ligand species to signal through distinct receptor complexes, it is possible that changing the relative stoichiometry of different monomers alters the true phenotypic consequences. Moreover, *in situ* localization studies are most often done using ectopically expressed BMP proteins which could alter dimer composition, as well as saturate any regulatory proteins and different receptor complexes.

Here, we combined precise endogenous tagging and direct protein manipulation to explore the distribution, regulation, and function of homo- and heterodimers in the *Drosophila* wing disc. We show that despite their distinct gene expression patterns, both Gbb and Dpp form strikingly similar extracellular gradients. This phenomenon reflects our finding that Gbb depends on Dpp for secretion. Furthermore, our use of extracellular membrane tethering via protein binders demonstrate that Gbb and Dpp are physically linked in the extracellular space, strongly indicative of heterodimer formation. The same experimental approach failed to detect extracellular homodimers in wild type discs. However, in the

absence of endogenous Gbb, Dpp homodimers are detected. Together, our results provide strong evidence that a Dpp/Gbb heterodimer is the prevalent bioactive BMP ligand during wing disc development.

Results

Endogenous tagging of BMP ligands reveals coincident extracellular gradients of Dpp and Gbb

To visualize endogenous ligands *in situ*, we used CRISPR/Cas9 editing to introduce small epitope tags into the open reading frame of the endogenous *gbb* locus. Previous attempts to tag BMPs with bulky fluorescent proteins have been shown to result in partial loss of function [22]. Hence, we knocked-in the short tags HA and OLLAS using ssDonor templates (Fig 1A, Supp Fig 1A and STAR Methods). We also generated a double-tagged *OLLAS:HA:gbb* using the SEED/Harvest technology [23] (Supp Fig 1B and STAR Methods). To visualize Dpp, we made use of a recently generated *HA:dpp* allele [22] and generated an *OLLAS:dpp* version using the same approach as originally employed for *HA:dpp* generation (see STAR Methods). All tags were introduced immediately after the most C-terminal proconvertase cleavage site, in the ligand domain (Fig 1B). Adult wings of all the alleles generated did not present any morphological defects in homozygosity (Supp Fig 1C).

Consistent with previous reports [14], immunohistochemical detection of Dpp and Gbb using HA-tagged forms resulted in somewhat complementary patterns in the third instar imaginal wing disc (Fig 1C), with HA:Gbb being reduced in the stripe of cells that express HA:Dpp. In contrast to Gbb protein distribution, *gbb* is expressed uniformly as revealed by using a *gbb*-LacZ transcriptional reporter (Fig 1D), confirming previous *in situ* hybridization results [14]. The reduction in Gbb protein compared to *gbb* gene expression levels within the *dpp* expression domain might reflect a post-transcriptional or post-translational process.

Standard immunohistochemistry makes use of permeabilizing agents revealing the localization of both intra- and extracellular proteins. As most of Dpp in third instar wing discs is located intracellularly [24], the presence of low extracellular Dpp levels may be difficult to detect using standard protocols. Eliminating the permeabilization step in standard immunostaining protocols allows for the detection of extracellularly proteins (see STAR Methods). Using this approach, we found that extracellular HA:Dpp and HA:Gbb exhibit a remarkably similar graded distribution, with maximal levels adjacent to the anterior/posterior boundary (Fig 1 E). High-resolution imaging of extracellular OLLAS:Dpp and HA:Gbb showed considerable colocalization of these BMPs in the extracellular space (Fig. 1F, Supp Fig 2A and B). This high degree of extracellular co-localization, comparable to the double immunostaining of OLLAS:HA:Gbb (Supp Fig 2A’ and B’), raised the possibility that the predominant form of secreted BMP ligand is a Dpp-Gbb heterodimer.

Gbb secretion is dependent on Dpp

BMP proproteins dimerize in the ER of the cells that produce them; therefore, we expect the formation of Dpp-Gbb heterodimers to be limited to those cells in which both genes are expressed. We aimed at determining the source of extracellular Gbb by knocking-down *gbb*

expression in either posterior compartment cells by expressing a *gbb*RNAi under the control of the *hh*-Gal4 driver, or in the stripe of cells anterior to the A/P boundary, using *ptc*-Gal4 (Figure 2A). While *gbb* knock-down in the posterior compartment did not alter the graded profile of extracellular HA:Gbb, removing it from the anterior stripe abolished gradient formation (Figure 2A'). Thus, extracellular Gbb is predominately secreted by anterior stripe cells. Supporting the importance of stripe-derived Gbb, and in agreement with previous reports [21], *gbb*RNAi expression in the anterior compartment using *ptc*-Gal4 resulted in nonautonomous growth and patterning defects (Supp Fig 3A). *gbb*RNAi expression in the posterior compartment using *hh*-Gal4 led to the loss of the posterior cross vein (Supp Fig 3B).

Given the restricted expression of *dpp* in the anterior stripe of cells, we hypothesized that Dpp might be involved in Gbb secretion. We tested this hypothesis by knocking down *dpp* expression in the dorsal compartment with *dppRNAi* driven by the dorsal driver ap-Gal4 over a period of 18h using a thermo-sensitive Gal80 (longer depletion of *dpp* dramatically altered tissue size and morphology). *dpp* knockdown in the cells of the dorsal compartment strongly reduced or abolished extracellular Gbb when compared to ventral cells (Fig 2B). This reduction was accompanied by an increase in intracellular Gbb levels (Fig 2B), a buildup reflecting the failure of Gbb to be secreted in the absence of Dpp. The coincident increase of intracellular Gbb and loss of extracellular Gbb was only seen when *dpp*RNAi was expressed in a domain overlapping with the anterior stripe, the domain of endogenous *dpp* expression; no effect was observed when using the posterior driver *hh*-Gal4 (Supp. Fig 3C, D).

We then tested whether the expression of *dpp* was sufficient to trigger ectopic Gbb secretion. Overexpression of *dpp* in the dorsal compartment resulted in a large increase in extracellular secretion of endogenous HA:Gbb from all dorsal cells, creating an ectopic gradient invading the ventral compartment (Fig 2C). In the same genotype, we observed a profound reduction of the intracellular levels of HA:Gbb (Fig 2C). Similar results were obtained when *dpp* was overexpressed in the posterior compartment of the wing disc using *hh*-Gal4 (Supp. Fig 3E). The lower level of HA:Gbb seen in the anterior stripe of wild type discs was higher than that seen in cells when *dpp* was overexpressed, suggesting that intracellular Gbb is normally in excess and the level of Dpp determines how much Gbb is secreted. In both *dpp* knockdown and overexpression, *gbb* gene expression remained unaltered (Supp. Fig 3F).

Consistent with a hypothesis of intracellular ligand retention, HA:Gbb colocalized with an ER marker [25] in both anterior and posterior compartments (Fig 2D, Supp Fig 2C, D). The level of posterior HA:Gbb in ER positive structures was higher than HA:Gbb in the anterior stripe (Fig 2D).

Extracellular probing of BMPs reveals the existence of heteromeric ligand complexes

Collectively, our results are consistent with the hypothesis that Dpp and Gbb form heterodimers, given that both exhibit a similar extracellular distribution and that the presence of Dpp is associated with increased extracellular Gbb. Tools to directly detect the presence of heterodimers *in situ* have been lacking. Therefore, to interrogate the possible direct physical interaction between Dpp and Gbb in the extracellular space, we designed an assay

utilizing HATrap, a synthetic membrane-tethered receptor that can bind and trap secreted HA-tagged proteins with high affinity on the cell surface [22].

We predicted that when expressed in posterior cells (Figure 3A), HATrap would bind and accumulate extracellular HA-tagged peptides at the cell surface (Fig 3B). If the bound extracellular HA-tagged peptides originated from cells of the anterior stripe, they would be trapped and concentrated adjacent to the A/P compartment boundary (Fig 3B).

We first tested the ability of HATrap to accumulate an endogenously expressed, double-tagged OLLAS:HA:Dpp. The use of a double-tagged version is essential for this particular experiment, since the trapping via a given tag prohibits the use of this tag for antibody detection see: [23]. Consistent with previous reports [22], HATrap expression in posterior cells resulted in a strong extracellular accumulation of Dpp just posterior to the A/P boundary, as revealed by anti-OLLAS staining (Fig 3C). Similarly, posteriorly expressed HATrap led to the accumulation of extracellular, double-tagged OLLAS:HA:Gbb, again adjacent to the A/P boundary, strikingly similar to that observed for OLLAS:HA:Dpp, despite the fact that OLLAS:HA:Gbb is expressed throughout the posterior compartment (Fig 3D). As shown in Supp Fig 4A, expression of HATrap masks HA:Gbb when standard immunostaining is performed. One could thus surmise that HATrap could artefactually disrupt the regulated secretion of OLLAS:HA:Gbb when expressed in the same cells; alternatively, the presence of intracellular OLLAS:HA:Gbb could retain HATrap inside the cell, thereby reducing its concentration on the cell surface. The fact that OLLAS extracellular staining was not seen through the entire posterior compartment when OLLAS:HA:Gbb was trapped with HATraping (Fig 3D) indicates that HATrap is not facilitating Gbb secretion. The fact that the band of heightened OLLAS signal is broader than when OLLAS:HA:Dpp is trapped could reflect a reduction in the level of HATrap at the cell surface due to intracellular retention by OLLAS:HA:Gbb.

To test more directly for the presence of heterodimers or, more precisely, for the presence of physically linked Dpp-Gbb molecules, we asked whether trapping of HA:Gbb would lead to an accumulation of OLLAS:Dpp using the set-up described above. HATrap was expressed in posterior cells under the control of *hh-Gal4* in animals with the endogenous *gbb* locus tagged with HA (HA:*gbb*) and the endogenous *dpp* locus tagged with OLLAS (OLLAS:*dpp*), both in heterozygous conditions. Extracellular immunostaining for OLLAS revealed a band of high signal just posterior to the A/P boundary, showing that trapping of HA:Gbb resulted in an accumulation of OLLAS:Dpp which was most likely produced by the anterior stripe cells (Fig 3E). The reverse experiment, using HA:Dpp and OLLAS:Gbb in the presence of posterior HATrap, produced a similar band of high OLLAS signal. The trapping of HA:Dpp originating from the anterior stripe resulted in the accumulation of OLLAS:Gbb in posterior cells abutting the A/P boundary (Fig 3F). These results provide strong *in situ* evidence that these two BMPs travel together in the extracellular space. To further confirm that the origin of these ligands is indeed the anterior stripe, we expressed HATrap in the posterior compartment using *hh*-LexA in an HA:*dpp*, OLLAS:*gbb* background. In addition, we simultaneously knocked-down *gbb* from the anterior stripe by expressing *gbb*RNAi using *ptc*-Gal4. In contrast to the posterior OLLAS:Gbb accumulation seen in the control,

knockdown of stripe-derived *gbb* led to loss of OLLAS:Gbb accumulation in posterior cells (Supp Fig 4B).

The simplest explanation for our observations is that stripe-derived Gbb and Dpp are part of the same complex, forming a Cystein-linked heterodimer. While extracellular heterodimers may be the most plausible explanation, we cannot formally exclude the possibility that our results reflect higher order multimers, or that Gbb homodimers and Dpp homodimers share a common carrier that allows both ligands to be trapped by HATrap.

We further characterized the signaling capacity of trapped ligands by monitoring phosphorylated Mad (pMAD) in all the above conditions. We found that even in the presence of an untagged copy of the ligand (HA:*dpp*/+ or OLLAS:HA:*dpp*/+), trapping of HA:Dpp on the surface of posterior cells results in a partial loss of signaling (Supp Fig 5A, G), suggesting that HA binding via the trap partially impairs signal transduction. In contrast, HATrap expression in the posterior compartment in an HA:*gbb*/+ or OLLAS:HA:*gbb*/+ background resulted in a slight increase of pMad levels in the posterior cells (Supp Fig 5C, E), suggesting that HA:Gbb binding via the HATrap permits a certain degree of signaling. In either case, these manipulations only resulted in slight changes of the posterior compartment of the resulting adult wing (Supp Fig 5B, D, F, H).

BMP homodimers are not detected under physiological conditions

We made use of the same HATrap assay to interrogate the existence of homodimers. To that end, we generated transheterozygous animals that had one *dpp* allele tagged with HA and the other tagged with OLLAS. If homodimers form, the posterior expression of HATrap should result in an accumulation of OLLAS:Dpp (Figure 4A). However, we did not detect an accumulation of OLLAS:Dpp in posterior cells (Fig 4A' and A''), showing that under physiological conditions we are unable to detect homodimers. Moreover, this negative result increases confidence that the physical interaction of Dpp and Gbb observed in the experiments described above results from heterodimerization and that higher order multimers are a less likely explanation. In these experiments, and as observed when trapping HA:Dpp in other conditions (see Supp Fig 5A and G), pMad intensity was reduced (Supp Fig 6A). Likewise, adult wings did not show major size differences between compartments (Supp Fig 6B). We then tested for the presence of Gbb homodimers using the same approach, producing transheterozygous flies carrying a *HA:gbb* and *OLLAS:gbb* alleles. No extracellular accumulation of OLLAS:Gbb could be observed upon HATrap expression in the posterior cells (Supp. Fig. 7A). This is consistent with the model that Gbb secretion from the stripe is induced directly by heterodimerization with Dpp, and not indirectly by the stimulation of homodimer secretion.

While loss of *dpp* results in dramatic wing defects [17,18], loss of *gbb* has been associated with comparatively minor defects in patterning and growth [14]. This seems to contradict our results, as they suggest that heterodimers are the only bioactive form present in the wing imaginal discs. We hypothesize that the reduced defects in growth displayed by *gbb* mutants are due to compensatory signaling via the Dpp homodimer formed only under such conditions. We tested this hypothesis by trapping Dpp homodimers in the presence and absence of *gbb* expression. To do so, we had to make use of both Gal4/UAS and

LexO/LexA expression systems in order to simultaneously express HATrap in posterior cells and *gbb*RNAi in the anterior stripe (Fig. 4B). This setup resulted in the accumulation of OLLAS:Dpp in an *OLLAS:dpp/HA:dpp* background (Fig. 4B' and B''), demonstrating that Dpp homodimers are formed in the absence of Gbb, but not in the presence of Gbb (see above).

In order to test whether Gbb homodimers were produced in the absence of Dpp, we trapped HA:Gbb in the presence of OLLAS:Gbb while simultaneously knocking down *dpp* in the anterior stripe (with an 18h expression pulse). In these conditions, OLLAS:Gbb did not accumulate in posterior cells (Supp. Fig. 7B). This result indicates that, in contrast to Dpp, Gbb homodimers are not detected extracellularly in the absence of Dpp.

These results are consistent with our conclusion that, under endogenous physiological conditions, Gbb:Dpp heterodimers are the predominant bioactive ligand in the wing disc.

Moreover, the different secretion properties of Dpp and Gbb reconciles our results with the stronger wing phenotypes of *dpp* loss of function compared to *gbb* loss of function.

Direct manipulation of Gbb results in stronger phenotypes than genetic loss.

Our data supports that the Gbb/Dpp heterodimers are the main bioactive ligand in the wing disc, Dpp homodimers only being produced upon loss of *gbb*. A direct prediction of this model would be that the genetic loss of *gbb* should produce milder phenotypes than interfering with Gbb at the protein level, once the heterodimers have formed. Direct interference with the heterodimer would not allow for the formation of Dpp homodimers, as it happens upon genetic *gbb* loss. HATrap has recently been used to investigate the importance of Dpp dispersal for wing formation [22]. In this case, HATrap was used to trap *HA:Dpp* on the membrane of Dpp producing cells in an homozygous HA:dpp background. This manipulation greatly perturbed signaling in the posterior compartment while the anterior signaling remained largely unaffected [22].

In the same fashion, we expressed HATrap using the *ptc*-Gal4 driver in an *HA:gbb* homozygous background. This manipulation resulted in strong reduction of the overall pMad signal, with low levels in the anterior stripe and very little signal in the posterior compartment (Fig 5A). We compared this manipulation with genetic loss by knocking-down *gbb* expression with an RNAi also driven by the *ptc*-Gal4 driver. In this condition, pMad was severely affected with overall reduction in the wing pouch and a narrow peak in the posterior compartment (Fig 5B) as seen when null clones of *gbb* encompass the entire anterior compartment [21]. Interestingly, the effect on the posterior pMad is stronger when trapping HA:Gbb than when gbb is knocked down (compare Fig 5A and B). Despite the stronger reduction in posterior pMad intensity when trapping HA:Gbb versus *gbb* knock-down (Fig 5A and B), the resulting adult wings displayed stronger defects in the vein L5 patterning upon RNAi expression than upon HA:Gbb trapping (Supp fig 8A). We suspected that the comparatively mild phenotype could arise due to partially "insufficient" trapping. We have previously suggested that a good practice to test the trapping "efficiency" is to reduce the ligand dose by half using a hemizygous background [26]. In these lines, HATrap expression in the anterior cells via *ptc*-Gal4 in the hemiyzgous HA:*gbb/gbb*^{1} background presented

comparatively stronger phenotypes than those seen when trapping in homozygous HA:*gbb* animals (Supp Fig 8B), and were highly similar to those seen upon *gbb*RNAi expression (Fig 8A' and B'). This suggest that not all secreted HA:Gbb molecules are bound, probably due to the relative expression levels of Gbb and the HATrap. In agreement with this interpretation, the trapping efficiency was further increased by doubling the genetic dosage of the UAS-HATrap transgene or both the UAS-HATrap and the *ptc*-Gal4 driver, resulting in further reduced pMad levels and reduced wing disc size (Supp Fig 8C). Unfortunately, these stronger disc phenotypes could not be further analyzed in the adult wing, as the animals died in pupal stages.

Together, these results demonstrate that the direct Gbb protein manipulation results in stronger phenotypes than the genetic *gbb* loss. This suggests that the *gbb* genetic loss is rescued by a compensatory mechanism, most likely the ectopic production of Dpp homodimers.

Heterodimer formation ensures long range gradient formation

These newly gained insights permitted us to directly compare the heterodimer condition (wild type) versus an exclusive homodimer condition (*gbb* knock-down in the wing pouch, using *gbb*RNAi driven by *ptc*-Gal4). We evaluated the extracellular localization of OLLAS:Dpp in both cases in order to assess the distribution of endogenous ligand. Compared to the wild type OLLAS:Dpp extracellular gradient, formed by heterodimers, OLLAS:Dpp homodimers are distributed mainly in the central part of the wing pouch, forming a gradient with abrupt slopes and reduced range (Fig. 5C, Supp Fig 9A). The overall anti-OLLAS signal was comparable in both conditions, indicating that OLLAS:Dpp was secreted at similar levels in the absence of Gbb. These results demonstrate that the differences in signaling between the homo- and heterodimers cannot simply be explained by reduced ligand production and suggest that the Dpp-Dpp homodimer triggers signaling less efficiently than the Dpp-Gbb heterodimer. Similar changes in OLLAS:Dpp distribution were observed when *gbb* was knocked-down in the dorsal compartment (using in the *ap*-Gal4 driver) compared to the ventral compartment (Supp. Fig 9B). Signaling levels and patterning were also severely affected in this condition (Supp. Fig 9C).

Differential receptor usage of heterodimers and homodimers

Similar to other BMPs, Dpp and Gbb have been proposed to activate signaling through distinct receptor complexes [21,27,28]. However, the relative contribution of each receptor when binding either homo- or heterodimers has never been studied in detail. The wing imaginal disc expresses two genes encoding BMP type I receptors, Saxophone (Sax) and Thickveins (Tkv), and two genes encoding the type II receptors, Punt (Put) and Wishful thinking (Wit) [29–31]. The active signaling receptor is a heterotetramer composed of two type I and two type II subunits, therefore multiple receptor combinations are possible in the wing disc. We interrogated the requirement of specific receptors in heterodimer and homodimer conditions (Fig 6A). As described above, the Dpp-Gbb heterodimer is the only detectable form of dimeric ligand present in wild type discs. In turn, *gbb* knock-down results in the exclusive formation of Dpp homodimers. Thus, we knocked-down different receptors in the presence of Gbb ("Dpp-Gbb heterodimer background") or its absence ("Dpp homodimer

background") using the wing pouch driver *nub*-Gal4 (Fig 6B). We did not examine Tkv as its requirement for Dpp signal transduction is well established [32–34].

Consistent with previous reports [27], *sax* knock-down strongly affected pMAD amplitude (Fig 6C'). In contrast, when both *gbb* and *sax* were knocked-down, pMAD levels where not as reduced as seen in the *gbb* knock-down alone (compare Fig 6D' to Fig 6D). Instead, double *sax/gbb* knock-down provoked a mild signal enhancement (Fig. 6D'). This result suggests that, when Tkv is the only type I receptor expressed in the wing disc, Dpp homodimers elicit higher signaling. In support of this interpretation, the vein L4 defects caused by the *gbb* knock-down were partially rescued in the *sax- gbb* double knock-down (Fig 6H and H').

Knock-down of the Type II receptor *punt* also resulted in a dramatic reduction of pMAD levels (Fig 6C''), accompanied with a change in the shape of the pMad pattern, which became somewhat homogenous throughout the wing pouch. This pMAD levels were further reduced when both *gbb* and *punt* were knocked-down, resulting in an almost total loss of pMAD (Fig 6D''). These results suggest that Punt is necessary for reaching the highest pMAD levels by the Dpp-Gbb heterodimer and that it is required for the Dpp homodimer to elicit signaling.

Adult wing phenotypes of the *punt* knock-down resulted in miss-patterning of the veins (Fig 6G''), while the *punt*, *gbb* double knock-down resulted in almost total loss of the intervein regions between L3-L4 and between L4-L5 (Fig 6H'').

Taken together, our results suggest that in the wild-type wing, Dpp-Gbb heterodimers signal through a heterotetrametric complex composed of the type I receptors Tkv and Sax and the type II receptor Punt, with the possible contribution of another type II receptor. In the absence of Gbb, Dpp homodimers form receptor complexes composed by Tkv and Punt, with recruitment of Sax having a negative effect on signaling.

Discussion

BMP signaling is intrinsically combinatorial. At the base of this property is the ability of BMP ligands to form homo- and heterodimers. BMP heterodimers have been shown to be more potent signaling activators than homodimers in several contexts [7,9,35–37], probably due to the assembly of distinct receptor complexes [7]. Nevertheless, the different *in vivo* contribution of homo- and heterodimers remains in most cases obscure, mainly due to limitations of classical genetics to dissect *in vivo* dimer composition and/or contribution. In some scenarios, the existence of BMP heterodimers can be inferred by the similar phenotypes caused by the loss of the different ligands [28,38]. However, in most cases, both loss and gain of function genetic studies shift the stoichiometry between monomers contributing to the multimeric ligands, and thus fail to reveal the correct bioactive ligand under physiological conditions. In spite of these limitations, a role for heterodimers is suggested from the dominant phenotypes of certain BMP alleles [39–41] and by the genetic interactions between different BMP encoding genes [21,38]. Using new reagents coupled with extracellular immunohistochemistry, we examined the spatial distribution of Dpp and Gbb

in the Drosophila wing primordia and provide evidence that the predominant secreted BMP ligand in the wing imaginal disc is a Dpp/Gbb heterodimer. We propose a model by which the Dpp/Gbb heterodimer biogenesis is regulated (Fig 7A): Gbb is abundant and synthesized in all cells of the wing pouch. Only when co-expressed with Dpp it is it no longer retained in the ER, but secreted as a Dpp/Gbb heterodimer. Dpp, on the contrary, is not retained in the ER and is secreted even in the absence of Gbb. Heterodimerization is favored given the greater relative abundance of Gbb (Fig 2C). The localized expression domain of *dpp* and the regulated secretion of the Dpp/Gbb heterodimer provides a source of bioactive ligand that generates a graded signaling output (Fig 1E) mediated by heterotetrameric receptor complexes containing Sax, Tkv and Punt.

Our model can also explain the different phenotypes of *dpp* and *gbb* mutant wings. In *dpp* mutants, no bioactive BMP ligands is secreted, as Gbb secretion requires Dpp (Fig 7C). In *gbb* mutants, Dpp can form homodimers and activate signaling, albeit at altered levels and with altered distribution (Fig 4B and Fig 7B). Thus, the phenotype of *gbb* is milder than the phenotype of *dpp*, despite the fact that *in vivo*, all active ligands that we can detect in the wing imaginal disc are heterodimers.

Heterodimerization-dependent secretion

The idea of regulated heterodimer secretion has been proposed for another member of the TGF-ß superfamily. During early zebrafish embryogenesis, the Activin-like factors Nodal and Vg1 are required for mesoderm induction [42–44]. Vg1 cannot be processed nor secreted in the absence of Nodal [43]. Vg1 is only secreted in the cells where both Vg1 and Nodal are co-expressed. This observations and our model shed light on a conundrum: how can a ubiquitously localized factor, such as Gbb in the wing imaginal disc (Fig 1B) or Vg1 in the early zebrafish embryo [45,46], confer spatial information to a tissue? The mandatory requirement of heterodimer formation for secretion provides a satisfactory answer. While these factors are essential, it is their localized secretion governed by the formation of a heterodimeric ligand that enables patterning.

The regulated retention of Gbb remains to be explored. Vg1 monomer retention has been proposed to occur mainly through its pro-domain, through exposed cysteines, glycosylated asparagines, and BiP chaperone-binding motifs [47]. Only when heterodimerization occurs, processing is completed and secretion is initiated.

In the case of Gbb, it has been described that differential processing of the Gbb pro-protein by proconvertases depends on O-glycosylation [48] and at least in the wing disc, the mature ligand retains a large portion of the pro-domain attached to the mature ligand [48,49]. Moreover, cell culture experiments have shown that Gbb can be secreted upon co-expression of Dpp independently of its processing [48]. In other contexts, it has been proposed that certain factors can bind BMPs and regulate their secretion [50]. It could be that a similar factor exists in the wing disc to retain Gbb.

Signaling range and activity

Loss of *gbb* abrogates long-range BMP signaling in the wing disc [14,21]. This data led to the postulation that Dpp-Dpp homodimers could mediate short-range signaling, while Gbb-Dpp

and/or Gbb-Gbb homodimers would mediate long-range signaling [21]. The model presented here argues that the Gbb-Dpp heterodimers are the only bioactive BMP ligands in the wild type wing. Nevertheless, independently on their role under physiological conditions, both studies suggest that Dpp homodimers have limited range of activity. Here, we have measured the distribution of Dpp in the absence of *gbb* (Fig 5C). Our data suggest that Dpp-Dpp homodimers and Dpp-Gbb heterodimers differ both in their capacity to trigger signaling and in their dispersal properties. Differential distribution of homo- and heterodimers has been described in *Drosophila*, both in the early embryo and in the pupal posterior cross vein (PCV) [9,28,51]. In these cases, the differences of distribution have been explained by the existence of associated proteins that impact ligand distribution (Sog/Tsg in the early embryo and Sog/Cv in the PCV) that have different affinities for homo- and heterodimers [9,28]. Whether such mechanism exist in the wing disc during larval stages remains unexplored.

Differential receptor usage has been proposed to be at the heart of the differences in signaling activity displayed by distinct BMP dimers [7,52–54]. Here, we have dissected the contribution of the type I receptor Sax and the type II receptor Punt in the presence of homo- and heterodimers in the wing disc (Fig 6). Our results suggest that the heterodimers require Sax and Tkv to trigger highest signaling levels, whereas Sax is dispensable for signaling via Dpp homodimers. Indeed, the expression of Sax had a negative effect on the signaling output of homodimers. Interestingly, this scenario differs in other contexts, as it has recently been shown that during early zebrafish development, the homodimers of the Dpp ortholog BMP2 require two different type I receptors to signal (including the Sax homolog ACVR1) [52]. Type II receptor Punt was found to be required for maximum signaling of both hetero- and homodimers. While Punt is strictly required for signaling through homodimers, *punt* knockdown led to low, but persistent, signaling via heterodimers. This result could indicate that the heterodimers are able to recruit other type II receptors to the complex. Alternatively, it might reflect technical limitations in *punt* knockdown. These results support the notion that it is the context in which hetero- and homodimers are secreted and disperse, which will determine the differences in their signaling output.

Importance of endogenous tagging and protein binders.

Classical genetics has been key in revealing critical pathways and untangling biological systems. The power of loss and gain of function studies have permitted the functional dissection of numerous biological mechanisms. Yet, these approaches may fail to detect the contribution of specific players that are part of multimeric complexes and/or compensatory mechanisms. Here, we describe a paradigmatic example of such failings. For years, some studies assigned Gbb as having a minor role compared to Dpp in wing disc patterning and growth, based on its phenotypes and lower sensitivity to changes in gene dosage. Our data presented here demonstrates that under endogenous conditions, it is the synergistic action between both Dpp and Gbb that is critical for wild type wing patterning.

In recent years, the advent of CRISPR/Cas9 genome editing has cleared the way for efficient endogenous tagging of genes with unprecedented ease. Tagging not only permits the effective visualization and biochemical characterization of proteins, but also their direct *in situ* manipulation. To do so, genetically encoded tools based on protein binders have

been proposed [26,55–58]. These tools permit the acute manipulation of tagged proteins in predictable manners, thus opening the door for experiments that were, thus far, out of reach. With respect to the BMP pathway, the combination of endogenous tagging and protein binders has permitted the interrogation of Dpp dispersal [22,59], the construction of a minimal synthetic morphogen [60] and here, the detection of heterodimers. It is by combining these and other emerging tools with the power of genetics that we will better understand how proteins coordinate development.

Limitations of the study

The model of Dpp-dependent secretion of Gbb presented for the wing imaginal disc may not be generalizable to other contexts. Furthermore, the mechanism of heterodimerization has not been dissected biochemically, and the precise mechanism of Gbb retention and heterodimerization remains to be elucidated. With the provided in vivo results, it is not possible to conclude whether all the Gbb present inside the cells is in a monomeric form. However, Dpp overexpression is sufficient to promote Gbb secretion (Fig 2C), which suggests that ER-retained Gbb is competent to heterodimerize and is most likely stored in a monomeric form. We have only analyzed the role of Sax and Punt with respect to homo- or heterodimer signaling (Fig 6); the possible preferential usage of the other BMPR by the of homo- and heterodimers remains to be investigated.

STAR Methods

RESOURCE AVAILABILITY

Lead contact—Further information and requests for resources and reagents should be directed to and will be fulfilled by the lead contact, Markus Affolter (markus.affolter@unibas.ch).

Materials availability—Flies and plasmids are available from the lead contact.

Data and code availability—-No large-scale datasets have been generated in this study. The raw microscopy data that support the findings of this study are available from the lead author upon reasonable request. -Any additional information required to reanalyze the data shown in this paper is available from the lead contact upon request

EXPERIMENTAL MODEL AND SUBJECT DETAILS

Fly stocks and genetics—All flies used in this study were grown in regular polenta/ yeast vials and kept at 25°C unless specified. *sax*RNAi and *gbb*RNAi lines were validated in the wing disc (Supp Fig 10). The different fly stocks employed in this study can be found in the key resource table. The detailed genotype of each experiment included in main and supplementary figures can be found in the Supplementary Table 1.

METHOD DETAILS

Generation of different tagged *gbb* and *dpp* alleles—The *gbb* alleles were generated using CRISPR/Cas9. The tagging position for HA/OLLAS/OLLAS:HA knock-ins between the residues 351 and 352 of the *gbb* coding sequence was chosen based on the

tagging position described in Anderson & Wharton, 2017. gRNA target sites for this region were identified using the CRISPR Optimal Target finder (http://targetfinder.flycrispr.neuro.brown.edu/). The sequence of the sgRNA targeting the *gbb* locus was: 5' GCCCAACAACGTGCCGCTGC 3'. The gRNA was cloned by annealing of the following primer pair: 5` TGCAGCCCAACAACGTGCCGCTGC 3' and 5` AAACGCAGCGGCACGTTGTTGGGC 3' and restriction ligation into the pCFD5 vector according to [65]. Transgenic flies expressing the gRNA were established by injecting the resulting construct into P(CaryP)attP40 (BL 25709). To insert the HA-; and OLLAS-Tag, ssDNA donor templates of 120bps (HA-Tag: 5'-TATGTACAGGGTCTGCATCTGGCAGCTGCGGCCGCCTGCATAGTCCGGGACGTCATAGGGATAGCCGCCCGTGCTCTCCATCGGTTCTAGCAGCGGCACGTTGTTGGGCGACACCGACTTCT-3'; OLLAS-Tag: 5'-TATGTACAGGGTCTGCATCTGGCAGCTGCGGCCGCCTTTACCCATCAGGCGGGGTCCCAGCTCGTTCGCGAAGCCGCTGCCGCCCGTGCTCTCCATCGGTTCTAGCAGCGGCACGTTGTTGGGCGACACCGACTTCT-3') were ordered from Integrated DNA technologies. In both cases, the PAM sequence of the sgRNA target was changed from GGT to GAT to avoid cutting of the donor template.

To insert the OLLAS:HA-Tag, the SEED/Harvest Method [23] was employed. Briefly, a cassette including 185bp homology arms was synthesized and cloned by Genewiz into pUC-GW plasmid. Subsequently, the OLLAS:HA SEED cassette, including the selectable marker, was introduced into this vector according to the protocol proposed in: [23].

Nos-Cas9 flies (BL 54591) were crossed with P(*U6-gbb*.gRNA)attP40 males and injected with the ssDNA or SEED templates. All the survivors were crossed with gbb^{1}/CyO. From of the following F1 generation, several independent stocks were established with *Xa/Cyo*,RFP,*Tb*. Specifically, stocks that became homozygous were genotyped by Single Fly PCR in a subsequent step.

Integration of HA and OLLAS:HA was tested with the following primer pair: 5'TGCGGCCGCCTGCATAGTCC-3', 5'-CAAGTGGCTGACCGCC-3' Integration of OLLAS was tested with the following primer pair: 5'- TGCGGCCGCCTTTACCCATC-3'; 5'-CAAGTGGCTGACCGCC-3'

In both cases correct integration resulted in a PCR band of 500bps. SEED stocks were established following the crossing scheme reported in (Aguilar et al 2022).

OLLAS:*dpp* flies were generated as described for HA:*dpp* in Matsuda et al., 2021. Instead of an HA-tag, a fragment encoding for the OLLAS-tag was inserted between the XhoI and NheI sites in the plasmid pBS-attb-Dpp4.4 for injection. The resulting plasmid was injected into yw M(*vas*-int.Dm)zh-2A; $dpp^{MI03752}/Cyo$, P23. Transformants were screened and stocks were established again according to: [22].

Immunostainings and image acquisition—For a total antibody staining, third instar larvae were dissected in ice cold PBS (pH 7,2, Gibco™) and immediately fixed for 30 min, at room temperature (RT) in a paraformaldehyde solution (4% PFA in PBS). After fixation,

the larvae were extensively washed with PBST (0,3% Triton-X in PBS) to permeabilize the tissue. This was followed by a 1h incubation in blocking solution (5% Normal Goat Serum in PBST) at RT and a consequent primary antibody incubation at 4 °C over-night. Primary antibodies were diluted in blocking solution. The next day, the samples were washed 3×15 mins with PBST and incubated for 2 hours at RT with the secondary antibody solution. Samples were then washed 3×15 min with PBST, followed by 3×15min washes with PBS. Fixation, incubation and washing steps were performed with the samples gently rotating.

For extracellular stainings, larvae were dissected in cold S2 media, and incubated with the primary antibody for 1h on ice before fixation. Primary antibodies were diluted in blocking solution (5% NGS in S2 media). To guarantee thoroughly distribution of the antibody, samples were gently mixed by tapping at the tube tube every 10 minutes. Afterwards, the samples were washed at least 10x with PBS, followed by fixation (30min, 4% PFA in PBS). After permeabilization and blocking steps, performed as described above for total staining, either a new total antibody staining was conducted over-night, or the samples were incubated with secondary antibody at RT the same day.

For mounting of imaginal wing discs, samples were transferred to Vectashield, the desired tissues were separated from the rest of the larvae and placed on a glass slide. The samples were then covered with a cover slide and sealed using nail polish. Images were acquired with a Leica SP5 or a Zeiss LSM880 confocal microscope and analyzed using ImageJ.

QUANTIFICATION AND STATISTICAL ANALYSIS

Quantification of extracellular gradients and pMAD—Of each confocal image, an average projection was created by ImageJ using three sequential slices (Stacks → Z-Project). For each of these average projections a signal intensity profile along the A/P axis was created and collected in Excel. Alignment along the A/P compartment boundary was achieved based on an anti-Ptc staining. The average signal intensity profile of each experiment, consisting of intensity profiles of various wing imaginal discs, was created using the script wing_disc-alignment.py [22]. Different conditions were then compared using the script wingdisc_comparison.py. The resulting signal intensity profiles were visualized by Prism. Graphs comparing adult wing sizes indicate the mean with a red line. Statistical analyses were performed using Prism, all test were t-test unless specified. n numbers and p-values are specified in each figure legend.

Generation of colocalization maps and analysis—Images were acquired using the LSM880 confocal microscope in Airscan mode (63x objective, 2.7 zoom). Raw data was then processed using Zen black. Generated .czi files were then opened with ImageJ. Background was subtracted using the BackgroundSubtracter plugin to reduce experimental noise derived from immunostaining. Colocalization map was generated using the Coloc_map.groovy plugin, included in the IMCF_Utilities package. Colocalization analysis was performed using the imageJ plugin JACoP.

Supplementary Material

Refer to Web version on PubMed Central for supplementary material.

Acknowledgement

We would like to thank Prof. Alex Schier for comments. The work in the laboratory of M.A. was supported by grants from the Swiss National Science Foundation (310030_192659/1) and by funds from the Kanton Basel-Stadt and Basel-Land. GA and MB were supported by 'Fellowships for Excellence' from the International PhD Program in Molecular Life Sciences of the Biozentrum, University of Basel. KAW was supported by NIH R01-GM068118. SM was supported by SNSF Ambizione grant (PZ00P3_180019).

References.

1. Bragdon B, Moseychuk O, Saldanha S, King D, Julian J, and Nohe A. (2011). Bone Morphogenetic Proteins: A critical review. Cellular Signalling 23, 609–620. 10.1016/j.cellsig.2010.10.003. [PubMed: 20959140]
2. Wang RN, Green J, Wang Z, Deng Y, Qiao M, Peabody M, Zhang Q, Ye J, Yan Z, Denduluri S, et al. (2014). Bone Morphogenetic Protein (BMP) signaling in development and human diseases. Genes & Diseases 1, 87–105. 10.1016/j.gendis.2014.07.005. [PubMed: 25401122]
3. Miyazono K, Kamiya Y, and Morikawa M. (2010). Bone morphogenetic protein receptors and signal transduction. The Journal of Biochemistry 147, 35–51. 10.1093/jb/mvp148. [PubMed: 19762341]
4. Mishina Y, Suzuki A, Ueno N, and Behringer RR (1995). Bmpr encodes a type I bone morphogenetic protein receptor that is essential for gastrulation during mouse embryogenesis. Genes Dev 9, 3027–3037. 10.1101/gad.9.24.3027. [PubMed: 8543149]
5. Irish VF, and Gelbart WM (1987). The decapentaplegic gene is required for dorsal-ventral patterning of the Drosophila embryo. Genes & development 1, 868–879. [PubMed: 3123323]
6. Bach D-H, Park HJ, and Lee SK (2018). The Dual Role of Bone Morphogenetic Proteins in Cancer. Molecular Therapy - Oncolytics 8, 1–13. 10.1016/j.omto.2017.10.002. [PubMed: 29234727]
7. Little SC, and Mullins MC (2009). Bone morphogenetic protein heterodimers assemble heteromeric type I receptor complexes to pattern the dorsoventral axis. Nature Cell Biology 11, 637–643. 10.1038/ncb1870. [PubMed: 19377468]
8. Antebi YE, Linton JM, Klumpe H, Bintu B, Gong M, Su C, McCardell R, and Elowitz MB (2017). Combinatorial Signal Perception in the BMP Pathway. Cell 170, 1184–1196.e1124. 10.1016/j.cell.2017.08.015. [PubMed: 28886385]
9. Shimmi O, Umulis D, Othmer H, and O'Connor MB (2005). Facilitated Transport of a Dpp/Scw Heterodimer by Sog/Tsg Leads to Robust Patterning of the Drosophila Blastoderm Embryo. Cell 120, 873–886. 10.1016/j.cell.2005.02.009. [PubMed: 15797386]
10. Wang Y-C, and Ferguson EL (2005). Spatial bistability of Dpp–receptor interactions during Drosophila dorsal–ventral patterning. Nature 434, 229–234. 10.1038/nature03318. [PubMed: 15759004]
11. Nguyen M, Park S, Marqués G, and Arora K. (1998). Interpretation of a BMP Activity Gradient in Drosophila Embryos Depends on Synergistic Signaling by Two Type I Receptors, SAX and TKV. Cell 95, 495–506. 10.1016/S0092-8674(00)81617-7. [PubMed: 9827802]
12. Zecca M, Basler K, and Struhl G. (1995). Sequential organizing activities of engrailed, hedgehog and decapentaplegic in the Drosophila wing. Development 121, 2265–2278. 10.1242/dev.121.8.2265. [PubMed: 7671794]
13. Capdevila J, and Guerrero I. (1994). TARGETED EXPRESSION OF THE SIGNALING MOLECULE DECAPENTAPLEGIC INDUCES PATTERN DUPLICATIONS AND GROWTH ALTERATIONS IN DROSOPHILA WINGS. Embo Journal 13, 4459–4468. 10.1002/j.1460-2075.1994.tb06768.x. [PubMed: 7925288]
14. Khalsa O, Yoon JW, Torres-Schumann S, and Wharton KA (1998). TGF-beta/BMP superfamily members, Gbb-60A and Dpp, cooperate to provide pattern information and establish cell identity in the Drosophila wing. Development 125, 2723–2734. 10.1242/dev.125.14.2723. [PubMed: 9636086]
15. Nellen D, Burke R, Struhl G, and Basler K. (1996). Direct and Long-Range Action of a DPP Morphogen Gradient. Cell 85, 357–368. 10.1016/S0092-8674(00)81114-9. [PubMed: 8616891]

16. Lecuit T, Brook WJ, Ng M, Calleja M, Sun H, and Cohen SM (1996). Two distinct mechanisms for long-range patterning by Decapentaplegic in the Drosophila wing. Nature 381, 387–393. 10.1038/381387a0. [PubMed: 8632795]

17. Spencer FA, Hoffmann FM, and Gelbart WM (1982). Decapentaplegic: A gene complex affecting morphogenesis in Drosophila melanogaster. Cell 28, 451–461. 10.1016/0092-8674(82)90199-4. [PubMed: 6804094]

18. Teleman AA, and Cohen SM (2000). Dpp Gradient Formation in the Drosophila Wing Imaginal Disc. Cell 103, 971–980. 10.1016/S0092-8674(00)00199-9. [PubMed: 11136981]

19. Bosch PS, Ziukaite R, Alexandre C, Basler K, and Vincent J-P (2017). Dpp controls growth and patterning in Drosophila wing precursors through distinct modes of action. eLife 6, e22546. 10.7554/eLife.22546.

20. Barrio L, and Milán M. (2017). Boundary Dpp promotes growth of medial and lateral regions of the Drosophila wing. eLife 6, e22013. 10.7554/eLife.22013.

21. Bangi E, and Wharton K. (2006). Dpp and Gbb exhibit different effective ranges in the establishment of the BMP activity gradient critical for Drosophila wing patterning. Developmental Biology 295, 178–193. 10.1016/j.ydbio.2006.03.021. [PubMed: 16643887]

22. Matsuda S, Schaefer JV, Mii Y, Hori Y, Bieli D, Taira M, Plückthun A, and Affolter M. (2021). Asymmetric requirement of Dpp/BMP morphogen dispersal in the Drosophila wing disc. bioRxiv, 2020.2011.2023.394379. 10.1101/2020.11.23.394379.

23. Aguilar G, Bauer M, Vigano MA, Jiménez-Jiménez C, Guerrero I, and Affolter M. (2022). In vivo seamless genetic engineering via CRISPR-triggered single-strand annealing. bioRxiv, 2022.2006.2017.496589. 10.1101/2022.06.17.496589.

24. Romanova-Michaelides M, Hadjivasiliou Z, Aguilar-Hidalgo D, Basagiannis D, Seum C, Dubois M, Jülicher F, and Gonzalez-Gaitan M. (2022). Morphogen gradient scaling by recycling of intracellular Dpp. Nature 602, 287–293.10.1038/s41586-021-04346-w. [PubMed: 34937053]

25. Lajeunesse DR, Buckner SM, Lake J, Na C, Pirt A, and Fromson K. (2004). Three new Drosophila markers of intracellular membranes. BioTechniques 36, 784–790. 10.2144/04365ST01. [PubMed: 15152597]

26. Aguilar G, Vigano MA, Affolter M, and Matsuda S. (2019). Reflections on the use of protein binders to study protein function in developmental biology. Wiley Interdisciplinary Reviews: Developmental Biology. 10.1002/wdev.356.

27. Bangi E, and Wharton K. (2006). Dual function of the Drosophila Alk1/Alk2 ortholog Saxophone shapes the Bmp activity gradient in the wing imaginal disc. Development 133, 3295–3303. 10.1242/dev.02513. [PubMed: 16887821]

28. Shimmi O, Ralston A, Blair SS, and O'Connor MB (2005). The crossveinless gene encodes a new member of the Twisted gastrulation family of BMP-binding proteins which, with Short gastrulation, promotes BMP signaling in the crossveins of the Drosophila wing. Developmental Biology 282, 70–83. 10.1016/j.ydbio.2005.02.029. [PubMed: 15936330]

29. Brummel TJ, Twombly V, Marqués G, Wrana JL, Newfeld SJ, Attisano L, Massagué J, O'Connor MB, and Gelbart WM (1994). Characterization and relationship of dpp receptors encoded by the saxophone and thick veins genes in Drosophila. Cell 78, 251–261. 10.1016/0092-8674(94)90295-X. [PubMed: 8044839]

30. Childs SR, Wrana JL, Arora K, Attisano L, O'Connor MB, and Massagué J. (1993). Identification of a Drosophila activin receptor. Proceedings of the National Academy of Sciences 90, 9475–9479. 10.1073/pnas.90.20.9475.

31. Marqués G, Bao H, Haerry TE, Shimell MJ, Duchek P, Zhang B, and O'Connor MB (2002). The Drosophila BMP Type II Receptor Wishful Thinking Regulates Neuromuscular Synapse Morphology and Function. Neuron 33, 529–543. 10.1016/S0896-6273(02)00595-0. [PubMed: 11856528]

32. Ruberte E, Marty T, Nellen D, Affolter M, and Basler K. (1995). An absolute requirement for both the type II and type I receptors, punt and thick veins, for dpp signaling in vivo. Cell 80, 889–897. 10.1016/0092-8674(95)90292-9. [PubMed: 7697719]

33. Tanimoto H, Itoh S, ten Dijke P, and Tabata T. (2000). Hedgehog creates a gradient of DPP activity in Drosophila wing imaginal discs. Molecular Cell 5, 59–71. 10.1016/s1097-2765(00)80403-7. [PubMed: 10678169]
34. Schwank G, Dalessi S, Yang S-F, Yagi R, de Lachapelle AM, Affolter M, Bergmann S, and Basler K. (2011). Formation of the Long Range Dpp Morphogen Gradient. Plos Biology 9, e1001111. 10.1371/journal.pbio.1001111.
35. Hazama M, Aono A, Ueno N, and Fujisawa Y. (1995). Efficient Expression of a Heterodimer of Bone Morphogenetic Protein Subunits Using a Baculovirus Expression System. Biochemical and Biophysical Research Communications 209, 859–866. 10.1006/bbrc.1995.1578. [PubMed: 7733977]
36. Isaacs MJ, Kawakami Y, Allendorph GP, Yoon B-H, Belmonte JCI, and Choe S. (2010). Bone Morphogenetic Protein-2 and −6 Heterodimer Illustrates the Nature of Ligand-Receptor Assembly. Molecular Endocrinology 24, 1469–1477. 10.1210/me.2009-0496. [PubMed: 20484413]
37. Zhao M, Zhao Z, Koh J-T, Jin T, and Franceschi RT (2005). Combinatorial gene therapy for bone regeneration: Cooperative interactions between adenovirus vectors expressing bone morphogenetic proteins 2, 4, and 7. Journal of Cellular Biochemistry 95, 1–16. 10.1002/jcb.20411. [PubMed: 15759283]
38. Ray RP, and Wharton KA (2001). Context-dependent relationships between the BMPs gbb and dpp during development of the Drosophila wing imaginal disk. Development 128, 3913–3925. 10.1242/dev.128.20.3913. [PubMed: 11641216]
39. Ho AM, Marker PC, Peng H, Quintero AJ, Kingsley DM, and Huard J. (2008). Dominant negative Bmp5mutation reveals key role of BMPs in skeletal response to mechanical stimulation. BMC Developmental Biology 8, 35. 10.1186/1471-213X-8-35. [PubMed: 18380899]
40. Thomas JT, Kilpatrick MW, Lin K, Erlacher L, Lembessis P, Costa T, Tsipouras P, and Luyten FP (1997). Disruption of human limb morphogenesis by a dominant negative mutation in CDMP1. Nature Genetics 17, 58–64. 10.1038/ng0997-58. [PubMed: 9288098]
41. Kim H-S, Neugebauer J, McKnite A, Tilak A, and Christian JL (2019). BMP7 functions predominantly as a heterodimer with BMP2 or BMP4 during mammalian embryogenesis. eLife 8, e48872. 10.7554/eLife.48872.
42. Pelliccia JL, Jindal GA, and Burdine RD (2017). Gdf3 is required for robust Nodal signaling during germ layer formation and left-right patterning. eLife 6, e28635. 10.7554/eLife.28635.
43. Montague TG, and Schier AF (2017). Vg1-Nodal heterodimers are the endogenous inducers of mesendoderm. eLife 6, e28183. 10.7554/eLife.28183.
44. Bisgrove BW, Su Y-C, and Yost HJ (2017). Maternal Gdf3 is an obligatory cofactor in Nodal signaling for embryonic axis formation in zebrafish. eLife 6, e28534. 10.7554/eLife.28534.
45. Dohrmann CE, Kessler DS, and Melton DA (1996). Induction of Axial Mesoderm by zDVR-1, the Zebrafish Orthologue ofXenopusVg1. Developmental Biology 175, 108–117. 10.1006/dbio.1996.0099. [PubMed: 8608857]
46. Helde KA, and Grunwald DJ (1993). The DVR-1 (Vg1)Transcript of Zebrafish Is Maternally Supplied and Distributed throughout the Embryo. Developmental Biology 159, 418–426. 10.1006/dbio.1993.1252. [PubMed: 8405668]
47. Dingal PCDP, Carte AN, Montague TG, and Schier AF (2021). Regulation of Vg1 biogenesis during mesendoderm induction. bioRxiv, 2021.2004.2025.441333.10.1101/2021.04.25.441333.
48. Anderson EN, and Wharton KA (2017). Alternative cleavage of the bone morphogenetic protein (BMP), Gbb, produces ligands with distinct developmental functions and receptor preferences. Journal of Biological Chemistry 292, 19160–19178. 10.1074/jbc.M117.793513. [PubMed: 28924042]
49. Akiyama T, Marqués G, and Wharton Kristi A. (2012). A Large Bioactive BMP Ligand with Distinct Signaling Properties Is Produced by Alternative Proconvertase Processing. Science Signaling 5, ra28–ra28. 10.1126/scisignal.2002549. [PubMed: 22472650]
50. Wilkinson L, Kolle G, Wen D, Piper M, Scott J, and Little M. (2003). CRIM1 Regulates the Rate of Processing and Delivery of Bone Morphogenetic Proteins to the Cell Surface*. Journal of Biological Chemistry 278, 34181–34188. 10.1074/jbc.M301247200. [PubMed: 12805376]

51. Matsuda S, and Shimmi O. (2012). Directional transport and active retention of Dpp/BMP create wing vein patterns in Drosophila. Developmental Biology 366, 153–162. 10.1016/j.ydbio.2012.04.009. [PubMed: 22542596]
52. Tajer B, Dutko JA, Little SC, and Mullins MC (2021). BMP heterodimers signal via distinct type I receptor class functions. Proc Natl Acad Sci U S A 118. 10.1073/pnas.2017952118.
53. Shimmi O, Umulis D, Othmer H, and O'Connor MB (2005). Facilitated transport of a Dpp/Scw heterodimer by Sog/Tsg leads to robust patterning of the Drosophila blastoderm embryo. Cell 120, 873–886. 10.1016/j.cell.2005.02.009. [PubMed: 15797386]
54. Karim MS, Madamanchi A, Dutko JA, Mullins MC, and Umulis DM (2021). Heterodimer-heterotetramer formation mediates enhanced sensor activity in a biophysical model for BMP signaling. PLoS Comput Biol 17, e1009422. 10.1371/journal.pcbi.1009422.
55. Aguilar G, Matsuda S, Vigano MA, and Affolter M. (2019). Using Nanobodies to Study Protein Function in Developing Organisms. Antibodies 8, 16. 10.3390/antib8010016. [PubMed: 31544822]
56. Helma J, Cardoso MC, Muyldermans S, and Leonhardt H. (2015). Nanobodies and recombinant binders in cell biology. Journal of Cell Biology 209, 633–644. 10.1083/jcb.201409074. [PubMed: 26056137]
57. Xu J, Kim A-R, Cheloha RW, Fischer FA, Li JSS, Feng Y, Stoneburner E, Binari R, Mohr SE, Zirin J, et al. (2022). Protein visualization and manipulation in Drosophila through the use of epitope tags recognized by nanobodies. eLife 11, e74326. 10.7554/eLife.74326. [PubMed: 35076390]
58. Ingram JR, Schmidt FI, and Ploegh HL (2018). Exploiting Nanobodies' Singular Traits. In Annual Review of Immunology, Vol 36, Littman DR, and Yokoyama WM, eds. pp. 695–715. 10.1146/annurev-immunol-042617-053327.
59. Harmansa S, Hamaratoglu F, Affolter M, and Caussinus E. (2015). Dpp spreading is required for medial but not for lateral wing disc growth. Nature 527, 317–322. 10.1038/nature15712. [PubMed: 26550827]
60. Stapornwongkul KS, de Gennes M, Cocconi L, Salbreux G, and Vincent JP (2020). Patterning and growth control in vivo by an engineered GFP gradient. Science 370, 321–327. 10.1126/science.abb8205. [PubMed: 33060356]
61. Matsuda S, Aguilar G, Vigano MA, and Affolter M. (2022). Nanobody-Based GFP Traps to Study Protein Localization and Function in Developmental Biology. In Single-Domain Antibodies: Methods and Protocols, Hussack G, and Henry KA, eds. (Springer US), pp. 581–593. 10.1007/978-1-0716-2075-5_30.
62. González-Méndez L, Seijo-Barandiarán I, and Guerrero I. (2017). Cytoneme-mediated cell-cell contacts for Hedgehog reception. eLife 6. 10.7554/elife.24045.
63. Wharton KA, Cook JM, Torres-Schumann S, de Castro K, Borod E, and Phillips DA (1999). Genetic Analysis of the Bone Morphogenetic Protein-Related Gene, gbb, Identifies Multiple Requirements During Drosophila Development. Genetics 152, 629–640. 10.1093/genetics/152.2.629. [PubMed: 10353905]
64. Schindelin J, Arganda-Carreras I, Frise E, Kaynig V, Longair M, Pietzsch T, Preibisch S, Rueden C, Saalfeld S, Schmid B, et al. (2012). Fiji: an open-source platform for biological-image analysis. Nature Methods 9, 676–682. 10.1038/nmeth.2019. [PubMed: 22743772]
65. Port F, and Bullock SL (2016). Augmenting CRISPR applications in Drosophila with tRNA-flanked sgRNAs. Nature Methods 13, 852–854. 10.1038/nmeth.3972. [PubMed: 27595403]

Highlights

- Endogenous tagging combined with synthetic traps identify BMP dimer composition in situ
- Gbb secretion is dependent on Dpp expression
- Gbb/Dpp heterodimers are the only BMP ligands secreted in the imaginal wing disc
- Heterodimers trigger signaling at higher levels than would the Dpp homodimer

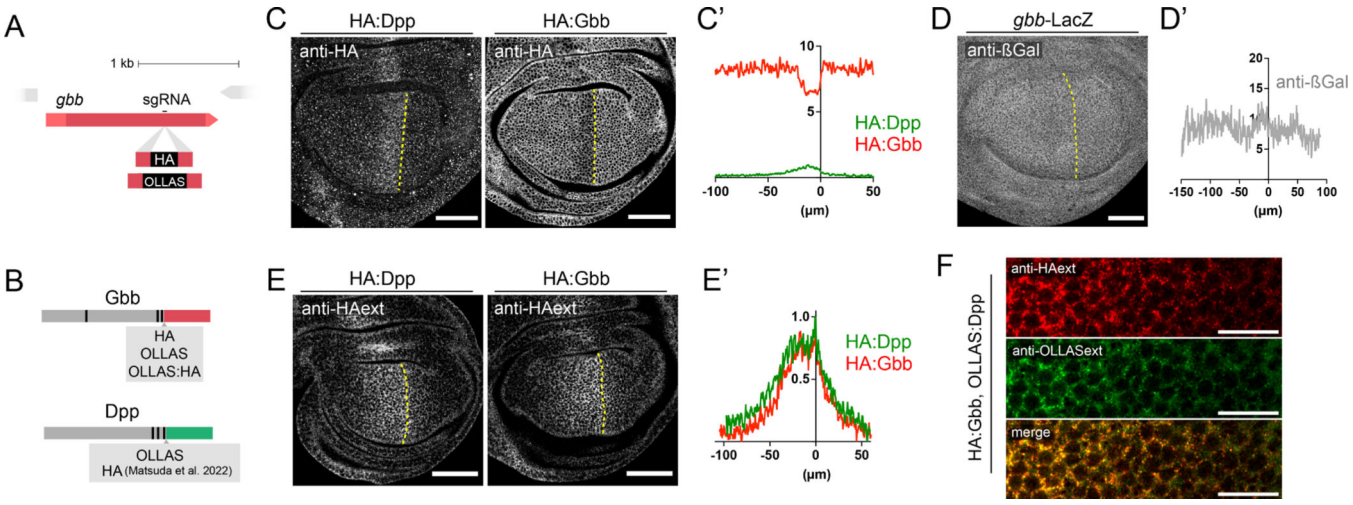

Figure 1: Endogenously tagged Gbb and Dpp form identical extracellular gradients. A. Outline of the sgRNA position to manipulate the *gbb* locus via the CRISPR/Cas9 system. **B.** Depiction of the tagging position in Gbb and Dpp. Both genes possess three pro-convertase cleavage sites in their prodomains. All tags were introduced after the last processing site in the beginning of the mature ligand domain (displayed in red for Gbb and green for Dpp). **C.** Conventional anti-HA antibody staining of homozygous HA:Dpp (left panel) and HA:Gbb (right panel) wing discs. HA:Dpp is expressed in a narrow stripe of anterior cells along the Antero/Posterior (A/P) compartment boundary. In contrast, HA:Gbb is uniformly detected in the whole wing disc, with a small decrease along the A/P boundary, in the same domain Dpp is expressed. **C'**. Fluorescent intensity profile of the panel C along the medio-lateral axis (HA:Dpp n=9, HA:Gbb =8). **D**. Anti-ßGal staining of *gbb*-LacZ reporter flies shows the uniform expression of *gbb* in the wing disc. **D**. Fluorescent intensity profile of the panel D along the medio-lateral axis (n=4) **E**. Extracellular anti-HA antibody stainings in homozygous HA:*dpp* and HA:*gbb* wing discs. Both HA:Dpp and HA:Gbb form an extracellular gradient, with peak values in the A/P border. **E'.** Quantification of the extracellular gradients of HA:Dpp (n=9) and HA:Gbb (n=8) shown in E along the medio-lateral axis. **F.** Simultaneous extracellular stainings of OLLAS:Dpp (green) and HA:Gbb (red) in the same wing disc. Co-localization of both ligands in the same image (Fake colour scale). Scale bars 50 μm except panel G (15 μm).

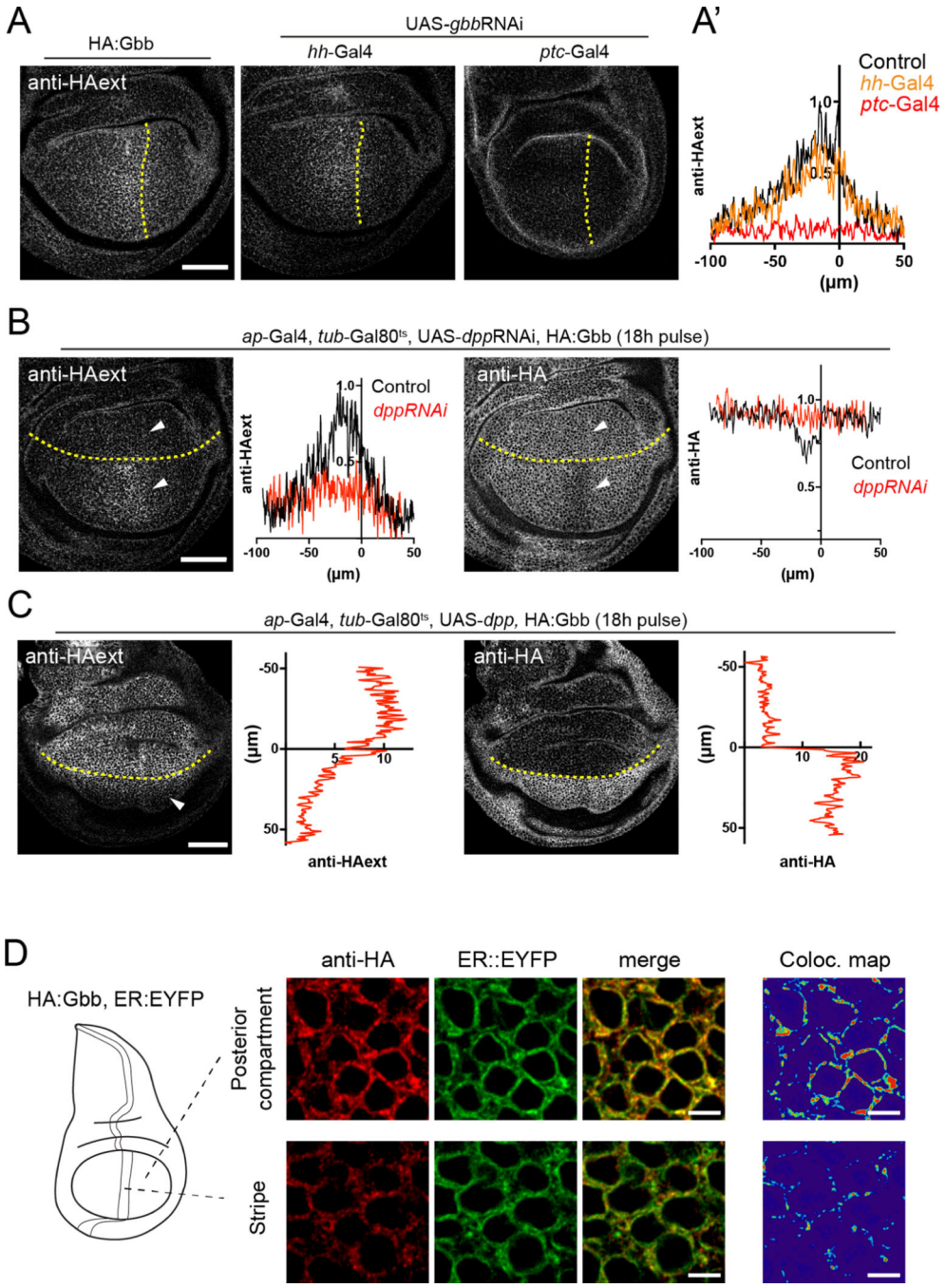

Figure 2: Gbb secretion is dependent on Dpp.

A. Anti-HA immunostaining in an HA:Gbb background in which *gbb*RNAi is expressed in different regions of the wing. Control HA:Gbb staining (left panel). Expression of *gbb*RNAi in the posterior compartment (using *hh*-Gal4) does not influence the extracellular HA:Gbb distribution (mid panel). Expression of *gbb*RNAi in the A/P stripe, the *dpp* expression domain, using *ptc*-Gal4, leads to a loss of the extracellular HA:Gbb gradient (right panel). **A'**. Quantification of the extracellular HA:Gbb staining along the medio-lateral axis with *gbb*RNAi expressed in different domains (control n=4; *hh*-Gal4 n=4; *ptc*-Gal4

n=6). **B.** Knock-down of Dpp by *dpp*RNAi in the dorsal compartment leads to a loss of extracellular HA:Gbb when expressed in the dorsal compartment using *ap*-Gal4 (right panel, see arrowheads pointing to both compartments). Total anti-HA staining of the same genotype. The reduction of HA:Gbb signal in the A/P stripe is no longer visible in the dorsal compartment (left panel, see arrows indicating both compartments). Quantifications of intra- and extra-cellular HA:Gbb distribution along the medio-lateral axis in the ventral and dorsal compartments (n=6). Larvae grew at 18°C and were transferred to 29°C 18h before dissection. **C.** Overexpression of Dpp in the dorsal compartment leads to massive HA:Gbb secretion from those cells (left panel), invading the ventral compartment (arrowheads). This leads to a nearly complete depletion of signal in immunostaining of total HA:Gbb in the dorsal compartment, much more pronounced than the reduction in the A/P stripe. Quantifications of intra- and extra-cellular HA:Gbb distribution along the proximo-distal axis, perpendicular to the dorsal-ventral boundary (n=6). Larvae were grown at 18°C and transferred to 29°C 18h before dissection. **D.** Subcellular localization of HA:Gbb in the different compartments and its colocalization with the ER marker sqh-EYFP:KDEL. Note that most of Gbb signal co-localizes in ER positive structures around the nuclei. Scale bars of panels A, B and C: 50 μm. Scale bar panel D: 3μm.

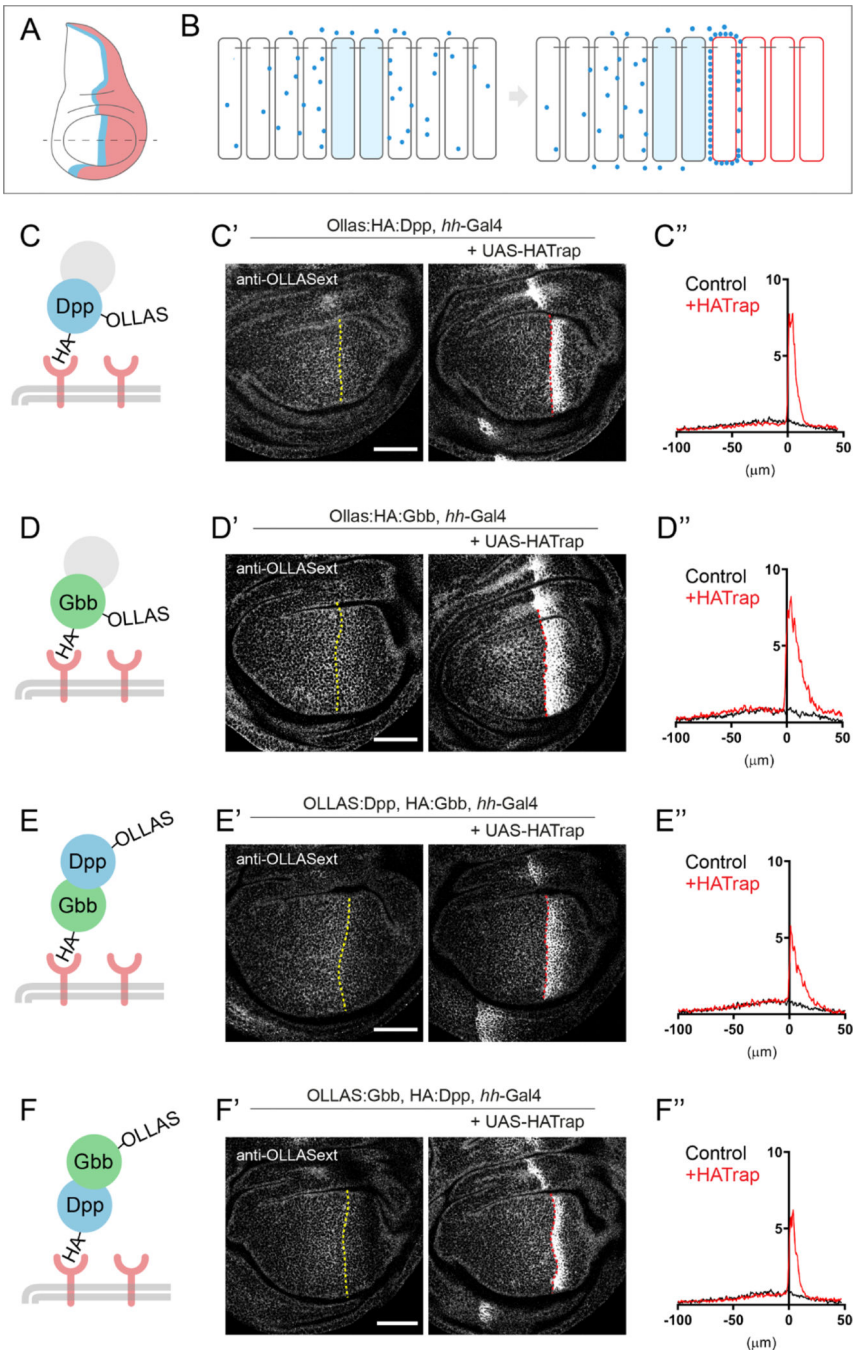

Figure 3: Extracellular tethering of BMP ligands reveals heterodimer existence

A-B. Schematic overview of the experimental set-up in the wing disc. **A.** Gbb and Dpp are both secreted from the anterior stripe of cells along the A/P compartment boundary (blue stripe). Expression of HA-Trap in the posterior compartment (labeled in red) could result in accumulation of stripe-derived HA-tagged ligands (for a review on the approach, see: [61]). **B.** In a wildtype tissue, BMP ligands are secreted from source cells and disperse distally, thereby creating an extracellular gradient. Expression of HATrap in the posterior compartment leads to accumulation, close to the stripe, of any HA-tagged

secreted peptide. **C.** Proof of principle of the system. Expression of HATrap with *hh*-Gal4 in an OLLAS:HA:Dpp background. OLLAS:HA:Dpp is strikingly accumulated when trap is expressed (right panel), when compared to when no trap is expressed (left panel), as revealed with anti-OLLAS staining. Accumulation occurs in the first few posterior cells adjacent to the A/P border (control n=7; HA-Trap n=7). Note: in this plot the graded nature of extracellular HA appears less dramatic when compared to Fig1E' or 2A' because the scale of the Y-axis must be extended to accommodate our measurements showing the higher level of ligands that accumulate in cells just posterior to the AP boundary upon HATrap expression. **D**. Likewise, OLLAS:HA:Gbb can be accumulated upon expression of HATrap by the *hh*-Gal4 driver. In spite of being expressed ubiquitously, OLLAS:HA:Gbb is only accumulated close to the stripe, indicating that only stripe-derived peptides are secreted, even if co-expressed with HATrap. Notice the broader accumulation respect panel C (control n=8; HATrap n=8). **E.** Trapping of HA:Gbb leads to an indirect accumulation of OLLAS:Dpp when HATrap is expressed in posterior cells via *hh*-Gal4 (control n=8; HATrap n=9). **F.** HA:Dpp trapping in posterior cells leads to an indirect accumulation of OLLAS:Gbb (control n=9; HATrap n=9). Scale bar 50 μm.

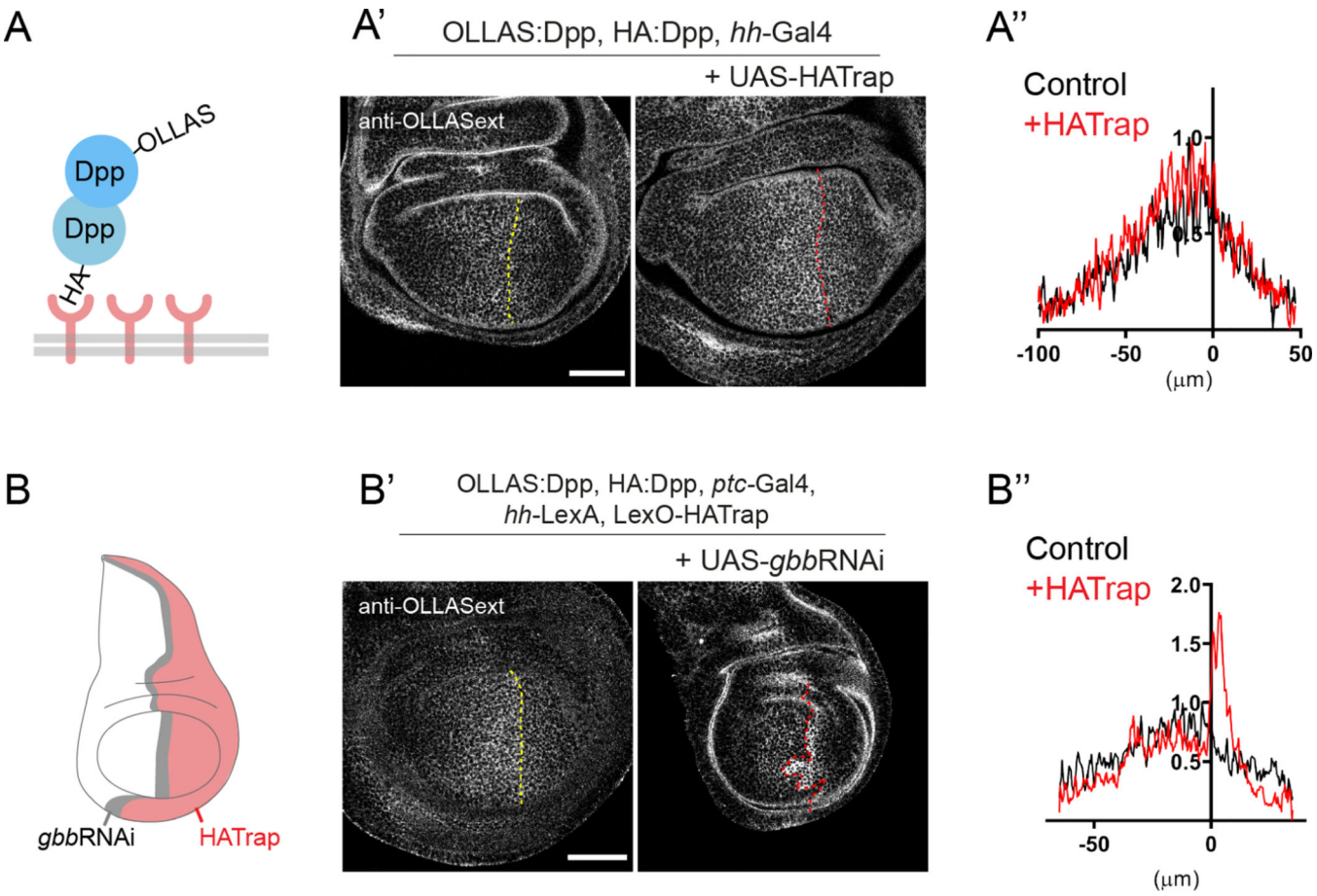

Figure 4: Dpp homodimers can only be detected in the absence of Gbb. A.
Scheme of the experiment in A'. HATrap is expressed in posterior cells using the *hh*-Gal4 driver in a background containing both HA:Dpp and OLLAS:Dpp. If homodimers exist, HA trapping should lead to OLLAS:Dpp accumulation. **A'.** Expression of HATrap in posterior cells does not lead to accumulation of OLLAS:Dpp (right panel) compared to control (left panel). **A''** Quantifications of extracellular OLLAS:Dpp in the absence and presence of HATrap (control n=5; HA-Trap n=7). **B.** Scheme of the experimental setup of B'. HATrap is expressed in the posterior compartment using *hh*-LexA while *gbb*RNAi is expressed in the anterior stripe using *ptc*-Gal4, in a HA:*dpp*, OLLAS:*dpp* background. **B'**. Expression of *gbb*RNAi leads to the indirect accumulation of OLLAS:Dpp when trapping HA:Dpp (right panel) compared to no *gbb*RNAi expression. **B''.** Quantifications of extracellular OLLAS:Dpp of the panels in B' (control n=6; HA-Trap n=7). Scale bars 50 μm.

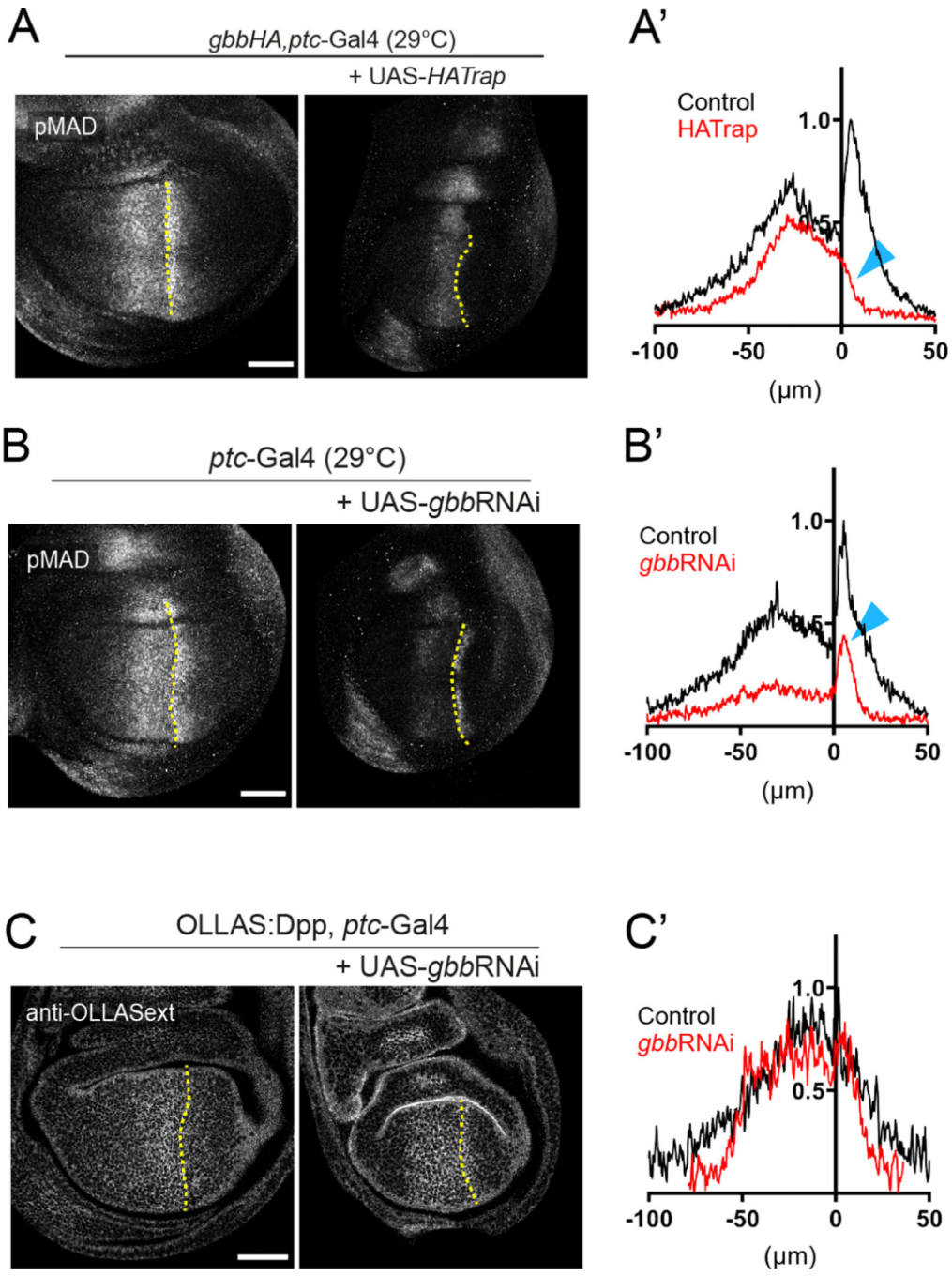

Figure 5: Dpp/Gbb heterodimers are functionally active and ensure long range gradient formation.

A. Trapping HA:Gbb on the membrane of Dpp-producing cells (via *ptc*-Gal4) leads to a strong reduction of pMAD signaling in the posterior compartment, while the anterior signal is still visible but restricted to the stripe (control n=9; HA-Trap n=13). **B.** Genetic knock-down of *gbb* using gbbRNAi driven by *ptc*-Gal4. pMAD is globaly reduced but the peak in the first cells of the posterior compartment is still visible (control n=7; gbbRNAi n=7). This posterior reduction is especially obvious in the quantification (blue arrows A' and

B'). Experiments in Figure 5A and B were conducted at 29°C. **C.** *gbb* knock-down in Dpp producing cells (via *ptc*-Gal4) compromises the extracellular OLLAS:Dpp gradient, leading to a reduction of long-range dispersal of OLLAS:Dpp (control n=9; gbbRNAi n=9). Scale bars 50μm.

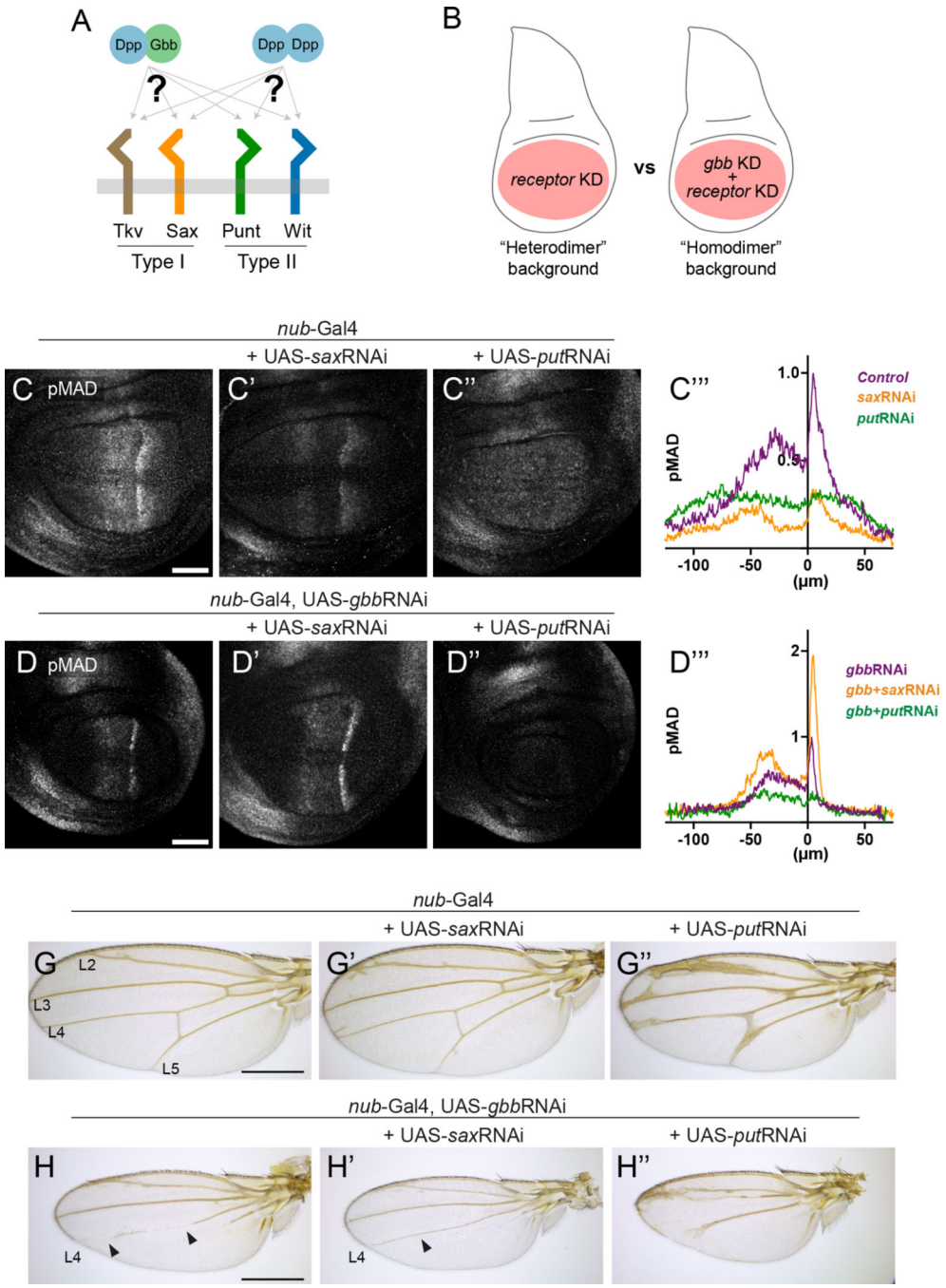

Figure 6: Heterodimer and homodimer use distinct receptors. A.
Gbb/Dpp heterodimers and Dpp homodimers potentially differ in their signaling output via different type I and type II receptor complexes in the wing disc. We tested the preferential usage of each receptor in a hetero- and homodimer environment. **B.** In a wildtype wing disc, Gbb/Dpp heterodimer are the only dimer form present, while removal of Gbb leads to a Dpp-homodimer environment. In these two conditions, the receptors Saxophone (Sax) and Punt (Put) were knocked-down by RNAi and the resulting pMAD signaling levels compared. **C.** Wild-type pMAD distribution in control discs. **C'.** pMAD distribution upon

*sax*RNAi expression using nub-Gal4 driver. pMAD amplitude is globally reduced, especially in the central stripe. **C’’.** pMAD distribution upon *put* knock-down. The characteristic “double peak” of pMAD distribution is lost and pMAD is instead rather homogeneous throughout the central pouch at low levels. **C’’’.** Quantification of the pMAD intensity profile along the medio-lateral axis in panels C, C’ and C’’ (control n=5, *sax*RNAi n=5, *put*RNAi n=7). **D.** pMAD distribution upon *gbb*RNAi expression using *nub*-Gal4 driver. Both pMAD intensity and range are reduced in comparison to a wildtype wing disc (as in C). **D’.** pMAD distribution upon double sax and *gbb* knock-down. Notice the slight increase in pMAD signal, especially obvious in the posterior peak. **D’’.** pMAD distribution upon double *put* and *gbb* knock-down. pMAD levels are practically undetectable in the pouch. **D’’’.** Quantification of the pMAD intensity profile along the medio-lateral axis in panels D, D’ and D’’ (*gbb*RNAi n=8, *gbb*+*sax*RNAi n=9, *gbb*+*put*RNAi n=6). **G**. Control adult wing phenotype. The minor L2 defects are common in *nub*-Gal4 transgenic flies. **G’.** Adult wing phenotype upon *sax* knockdown. Slightly bigger wings can be observed in comparison to the control displaying extra-vein tissue in the proximity of the longitudinal veins. **G’’.** Adult wing phenotype upon *put* knockdown. Wings are slightly reduced and display thickening of the longitudinal and cross veins. **H**. Adult wing phenotype upon *gbb* knockdown. Wings are considerably smaller in comparison to the control. The L5 is almost entirely lost while L4 presents severe defects. Cross veins are missing. **H’.** Adult wing phenotype upon double *gbb* and *sax* knockdown. Overall, this phenotype mimics that of single *gbb* knock-down (panel H) but the L4 defects are rescued. **H’’.** Adult wing phenotype upon double *gbb* and *put* knockdown. In this case, L2 and 4 are partially fused and L5 totally missing. No cross veins develop. Scale bars C and D: 50μm. Scale bars G and H: 500μm

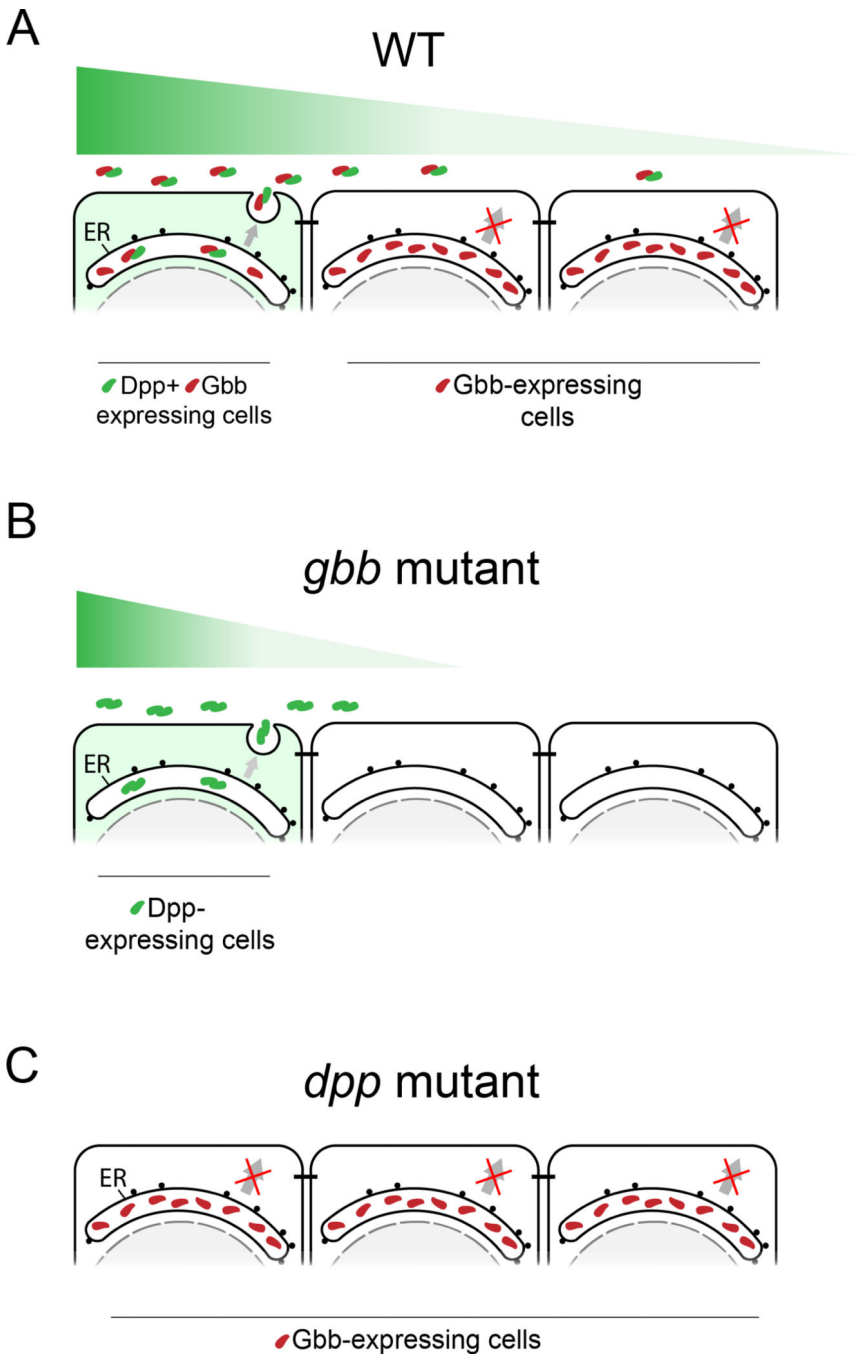

Figure 7. Model of Dpp/Gbb function in the imaginal wing disc.

A. In physiological conditions, Gbb is synthesized in all cells but retained in the ER. Only in the cells where Dpp is co-expressed (in green on the left), heterodimers will be formed. Heterodimers are the only bioactive form spreading from the stripe and will result in a long activity gradient. **B.** In absence of Gbb, Dpp will be able to form homodimers. However, these homodimers will have reduced dispersal and signaling capacities. **C.** In absence of

Dpp, Gbb will remain retained in the ER, no ligand is being secreted, resulting in total loss of BMP signal.

KEY RESOURCE TABLE

REAGENT or RESOURCE	SOURCE	IDENTIFIER
Antibodies		
anti-HA 3F10 (1:20 extracellular, 1:300 total)	Roche	Cat# 11867423001
anti-HA C29F4 (1:20 extracellular, 1:500 total)	Cell Signaling	Cat# 3724
anti-OLLAS L2 (1:20 extracellular)	Novus Biologicals	Cat# NBP1–06713
anti-phospho-Smad1/5 41D10 (1:200)	Cell Signaling	Cat# 9516
anti-Wg 4D4 (1:120)	DSHB	Cat# AB_528512
anti-Ptc (1:20)	DSHB	Cat# AB_528441
anti-β-Galactosidase (1:1000)	abcam	Cat# ab9361
goat anti-rat IgG Fc (FITC) (1:500)	abcam	Cat# ab97089
goat anti-rabbit IgG (H+L) Alexa Fluor 680 (1:500)	Thermo Fisher	Cat# A-21109
F(ab)2-goat anti-rabbit IgG (H+L) Alexa Fluor 568 (1:500)	Thermo Fisher	Cat# A-21069
goat anti-rabbit IgG (H+L) Alexa Fluor 488 (1:500)	Thermo Fisher	Cat# A-1108
goat anti-mouse IgG (H+L) Alexa Fluor 568 (1:500)	Thermo Fisher	Cat# A-11004
Alexa Fluor 680 AffiniPure goat anti-mouse IgG, Fcγ fragment specific (1:250)	Jackson ImmunoResearch	Cat# 115–625-071
IgY (H+L) Cross-Adsorbed goat anti-chicken, Alexa Fluor 488 (1:500)	Invitrogen	Cat# A32931
Bacterial and virus strains		
One Shot™ MIDDLE10 Electrocomp™ E. coli	Invitrogen	Cat# C404050
Chemicals, peptides, and recombinant proteins		
PBS pH 7.2 (1x)	gibco	Cat# 20012019
Schneider's Drosophila Medium (1x)	gibco	Cat# 21720024
Vectashield Antifade Mounting Medium	Vectorlabs	Cat# H-1000
Normal Goat Serum	Abcam	Cat# Ab7481
Paraformaldehyde 32%	Electron Microscopy Sciences	Cat# 157154
Triton X-100	Sigma Aldrich	Cat# T8787
Experimental models: Organisms/strains		
yw, HA:*dpp*	Matsuda et al. [22]	N/A
yw, OLLAS:*dpp*	This study	N/A
yw, OLLAS:HA:*dpp*	Matsuda et al. [22]	N/A
HA:*gbb*	This study	N/A
OLLAS:*gbb*	This study	N/A
OLLA:HA:*gbb*	This study	N/A
(y)w; gbb-lacZ/TM6Tb	Kristi Wharton, MCB Department, Brown University	N/A
ptc-Gal4	BDSC	BL207
hh-Gal4/*TM6Tb*	Gift from Manuel Calleja Centro de Biología	N/A

REAGENT or RESOURCE	SOURCE	IDENTIFIER
	Molecular, CSIC-UAM, Madrid, Spain	
nub-Gal4	Gift from Manuel Calleja Centro de Biología Molecular, CSIC-UAM, Madrid, Spain	N/A
hh-lexA	González-Méndez et al. [62]	N/A
DANN-*gbb*RNAi	BDSC	BL34898
DANN-*dpp*RNAi	BDSC	BL33618
DANN-*dpp*	BDSC	BL1486
ap-Gal	BDSC	BL3041
tubulin-Gal80^{ts}	BDSC	BL7016 BL7019 BL7017
UAS/LexAop-HATrap	Matsuda et al.[22]	
UAS-*sax*RNAi	VDRC	46350
UAS-*put*RNAi/*CyO*	BDSC	BL39025
P(*gbb* gRNA)attP40	This study	N/A
nos-Cas9	BDSC	BL54591
yw M{vas-int.Dm}zh-2A; dpp^{MI03752} /Cyo, P23	Matsuda et al. [22]	N/A
hsFLP; al, Pbac{RB}e00178 /SM6, al, sp	Matsuda et al. [22]	N/A
w[*] ; CyO, P{w[+mC]=2xTb[1]-RFP}CyO / T(2;3)ap[Xa]	BDSC	BL36336
gbb^{1} /CyO	Wharton et al. [63]	N/A
Oligonucleotides		
Oligo for gbb gRNA cloning Forward 5`TGCAGCCCAACAACGTGCCGCTGC 3'	Microsynth	N/A
Oligo for gbb gRNA cloning Reverse 5`AAACGCAGCGGCACGTTGTTGGGC 3'	Microsynth	N/A
HA-Tag ssDNA Donor 5'TATGTACAGGGTCTGCATCTGGCAGCTGCGGCC GCCTGCATAGTCCGGGACGTCATAGGGATAGCCG CCCGTGCTCTCCATCGGTTCTAGCAGCGGCACGTT GTTGGGCGACACCGACTTCT-3'	IDT	N/A
OLLAS-Tag ssDNA Donor 5'- TATGTACAGGGTCTGCATCTGGCAGCTGCGGCCG CCTTTACCCATCAGGCGGGGTCCCAGCTCGTTCGC GAAGCCGCTGCCGCCCGTGCTCTCCATCGGTTCTA GCAGCGGCACGTTGTTGGGCGACACCGACTTCT-3'	IDT	N/A
Forward oligo to confirm the insertion of HA in *gbb 5'- TGCGGCCGCCTGCATAGTCC-3'*	Microsynth	N/A
Reverse oligo to confirm the insertion of HA in *gbb 5'- CAAGTGGCTGACCGCC-3'*	Microsynth	N/A
Forward oligo to confirm the insertion of OLLAS in *gbb 5'- TGCGGCCGCCTTTACCCATC-3'*	Microsynth	N/A
Reverse oligo to confirm the insertion of OLLAS in *gbb 5'- CAAGTGGCTGACCGCC-3'*	Microsynth	N/A
Recombinant DANN		

REAGENT or RESOURCE	**SOURCE**	**IDENTIFIER**
pCFD5	Addgene	#73914
pBS-attb-Dpp4.4	Matsuda et al. [22]	N/A
Software and algorithms		
Fiji (imageJ)	64	https://imagej.nih.gov/ij/
Adobe Illustrator	Adobe	https://www.adobe.com/
GraphPad Prism 8	GraphPad Software	http://www.graphpad.com/
JACoB plugin	Bolte and Cordelières 2006	https://imagej.nih.gov/ij/plugins/track/jacop.html